

Thesis

THESIS  
OFO  
Car  
ACC  
Ph.D.

Accommodating lateral velocity variation  
AC .H3 no.C82 15267



Carter, Jerry A.  
SOEST Library

ACCOMODATING LATERAL VELOCITY VARIATIONS IN KIRCHHOFF  
MIGRATION OF ZERO OFFSET REFLECTION DATA

A DISSERTATION SUBMITTED TO THE GRADUATE DIVISION OF THE  
UNIVERSITY OF HAWAII IN PARTIAL FULFILLMENT  
OF THE REQUIREMENTS FOR THE DEGREE OF

DOCTOR OF PHILOSOPHY

IN GEOLOGY AND GEOPHYSICS

DECEMBER 1982

By

Jerry Allan Carter

Dissertation Committee:

Frederick K. Duennebier, Chairman  
L. Neil Frazer  
Don M. Hussong  
Ralph Moberly  
Dennis Moore  
Eduard Berg

We certify that we have read this dissertation and that in our opinion it is satisfactory in scope and quality as a dissertation for the degree of Doctor of Philosophy in Geology and Geophysics.

DISSERTATION COMMITTEE

Julius K. Dunbar  
Chairman

Dennis W. Moore

L. Neil Fray

Allen K.

John King

Robert Motley

## ACKNOWLEDGMENTS

I am indebted to several people for their help and support in bringing this dissertation to fruition. N.D. Whitmore of the Amoco Production Company provided the finite-difference synthetic reflection records used to test the migration routine and M.S. Redeker of Mobile Exploration Services Center provided the physical model data used to test the forward modeling program. The entire committee has been extremely patient with my unorthodox approach to meeting university requirements. Fred Duennebier in particular was very understanding in allowing me to pursue my ever-changing interests. My wife, Judy, has been a constant source of support, providing an extra measure of understanding that no one else could give. Finally, I would like to thank Neil Frazer for his guidance, time, and ideas which were invaluable to the completion of this dissertation.

## ABSTRACT

When velocity varies laterally as well as with depth an exact Kirchhoff depth migration requires that rays be traced from each depth point in the section to each source/receiver location. As such a procedure is prohibitively expensive, Kirchhoff migration is usually carried out by using a velocity function that depends only on depth. This dissertation introduces a new method, based on Fermat's principle, which is a compromise between these two extremes. The slowness (reciprocal velocity) function is written as the sum of two functions, the first of which is large and depends only on depth and the other of which is small and varies both with depth and position along the line. Raypaths are traced for the first slowness function and used to calculate migration curves. For each depth point these same raypaths are used to calculate travel time perturbations due to the laterally varying part of the slowness. The travel time perturbations are added to the migration curve to obtain an approximation to the exact migration curve. Migration is performed by summing over these curves with the proper weighting factors. Numerical tests have shown that this scheme works surprisingly well even when the lateral variation of velocity is large. This method may also be applied to the forward problem of modeling. In this application, energy at a point in the depth model is distributed over the migration curve in the synthetic time section rather than summed over one.



## TABLE OF CONTENTS

ACKNOWLEDGMENTS . . . . .	iii
ABSTRACT . . . . .	iv
LIST OF ILLUSTRATIONS . . . . .	vi
I. INTRODUCTION . . . . .	1
II. THEORY . . . . .	4
III. ACCOMODATING LATERAL VELOCITY VARIATIONS . . . . .	15
IV. EXAMPLES . . . . .	22
V. MODELING: THE FORWARD PROBLEM . . . . .	33
VI. FORWARD MODELING EXAMPLE . . . . .	39
VII. CONCLUSIONS . . . . .	45
REFERENCES . . . . .	47
APPENDIX A	
Notes on the real-time application of Kirchhoff migration . . . . .	49
APPENDIX B	
Rapid F-K migration of zero-offset marine reflection data . . . . .	52

## LIST OF ILLUSTRATIONS

Figure	Page
1 The integration volume and surfaces . . . . .	6
2 A ray tube from a point scatterer to the surface . . . . .	8
3 A comparison of rms and 10-ray interpolation migration curves . . . . .	14
4 Splitting the slowness-depth model . . . . .	16
5 Sample ray trace . . . . .	17
6 Coordinates for individual rays . . . . .	18
7 Determining perturbations to the reference model migration curves . . . . .	20
8 Example migration of finite difference synthetic data . . . . .	25
9 Example migration of finite difference synthetic data . . . . .	29
10 Diffraction curves are analogous to migration curves . . . . .	38
11 Comparison of physical model data to synthetic reflection section . . . . .	41

## I. INTRODUCTION

Migration has been an important technique in the processing of seismic reflection data ever since the pioneering work of Hagedoorn [1954]. Recent years have seen the development of computer-oriented migration methods based on the wave equation [e.g., Claerbout, 1970; Claerbout and Doherty, 1972; French, 1974; Gardner et al., 1974; Gazdag, 1978; Stolt, 1978]. Unfortunately, some of these methods are limited by the simple velocity-depth models which they must assume in order to be efficient. F-K migration [Stolt, 1978] assumes a constant velocity medium and can accommodate velocity variations only through pre-migration time-stretching techniques [Stolt, 1978] (see APPENDIX B). Gazdag's [1978] Fourier transform method uses the frequency and wavenumber domains to obtain accurate space derivatives but requires a transform at each depth, which makes it slow. The most widely used migration method, the finite difference method [Claerbout, 1970; Claerbout and Doherty, 1972], has proven to be one of the most accurate methods for handling complicated velocity-depth models but is also relatively slow. Kirchhoff migration [French, 1974; Schneider, 1978], which is the subject of this paper, is relatively rapid for a velocity function that varies only with depth and hitherto its use has been mostly limited to such models.

The conceptual basis of Kirchhoff migration and its relation to other migration methods has been treated in detail by French [1975]. In accordance with Claerbout's principle [Claerbout, 1971], each

subsurface point is assumed to be a point source and the velocity of the medium is assumed to be one-half the true velocity. As the source/receiver pair is moved along the surface, the reflections from a subsurface point form a diffraction pattern known as a migration curve. Summation over one such curve with the proper weighting function gives the value of the migrated section for that point. The collection of all of these summed points forms the migrated section.

The shape of the migration curve for a particular subsurface point depends on the velocity of the material above it. When velocity varies only with depth, the migration curves for all of the points at a particular depth are identical. Thus, Kirchhoff migration routines have traditionally assumed horizontally-independent velocity-depth models [e.g., French, 1974; 1975; Gardner et al., 1974; Schneider, 1978]. This assumption limits the effectiveness of these Kirchhoff schemes, as features related to horizontal velocity variations (e.g., velocity pull-ups) are not corrected. In order to properly migrate a section with lateral velocity variations, the migration curve for each subsurface point must be determined. An accurate but time-consuming method is to trace rays through a model of the section from each subsurface point to each surface offset.

In this paper we demonstrate a method of accommodating lateral velocity variations in a Kirchhoff migration scheme while avoiding most of the ray tracing that is necessary. This is accomplished by assuming a velocity-depth model that varies only with depth (reference model) for the ray trace as in conventional Kirchhoff migration, and

accomodating lateral velocity changes by approximating their effect with travel-time corrections to the migration curves generated using the reference model.

## II. THEORY

Previous derivations of the Kirchhoff integral are based on the assumption of a homogeneous medium [e.g., French, 1975; Schneider, 1978; Berkhout, 1981]. In this section we derive the Kirchhoff integral for a vertically inhomogeneous medium assuming coincident shot and receiver locations (i.e., single channel or stacked multichannel data). We begin with the Helmholtz equation,

$$(\nabla^2 + \omega^2/c^2) G = \delta(\underline{r} - \underline{r}_1) \quad (1)$$

in which  $G$  is the function which solves (1) and satisfies the radiation condition;  $\nabla^2$  is the Laplacian operator,  $\omega$  is frequency,  $c$  is velocity, and  $\delta$  is the Dirac delta function. Later,  $\underline{r}$  and  $\underline{r}_1$  will turn out to be the position vectors of the source/receiver pair and point scatterer, respectively. The wave field,  $\psi(\underline{r}, \omega)$ , satisfies the equation

$$(\nabla^2 + \omega^2/c^2) \psi(\underline{r}, \omega) = 0 \quad (2)$$

inside the volume  $V$  (Figure 1). To obtain the Kirchhoff integral, we use Green's second formula,

$$\int_V (\phi_1 \nabla^2 \phi_2 - \phi_2 \nabla^2 \phi_1) dV = \int_{\partial V} (\phi_1 \partial_n \phi_2 - \phi_2 \partial_n \phi_1) dA \quad (3)$$

where  $n$  is the outward normal to the surface  $\partial V$ , and substitute  $\phi_1 = \psi(\underline{r}, \omega)$  and  $\phi_2 = G$  to obtain

$$\psi(\underline{r}_1, \omega) = \int_{\partial V} \{ \psi(\underline{r}, \omega) \partial_n G - G \partial_n \psi(\underline{r}, \omega) \} dA, \quad (4)$$

which is the Kirchhoff integral.

French [1975] has shown that if the data are collected in a horizontal plane, the second term in the integrand of equation (4) is the negative of the first term. We therefore replace the second term containing the normal derivative of the data with the negative of the first term. Also, we extend the lower boundary of the integration surface to infinite depth so that by the radiation condition, the only remaining contribution to the integral comes from the surface  $S$  (Figure 1). Equation (4) thus becomes

$$\psi(\underline{r}_1, \omega) = 2 \int_S \psi(\underline{r}, \omega) \partial_n G dS. \quad (5)$$

We now write  $G = |G|e^{-i\omega\tau}$  and use the geometrical optics approximation for the amplitude  $|G|$  and phase  $\omega\tau$ . The negative sign in the phase of  $G$  is taken because we shall be extrapolating backward in time. Along a raypath, the variation in  $e^{-i\omega\tau}$  is much greater than the variation in  $|G|$ . Thus the first term in the derivative of  $G$

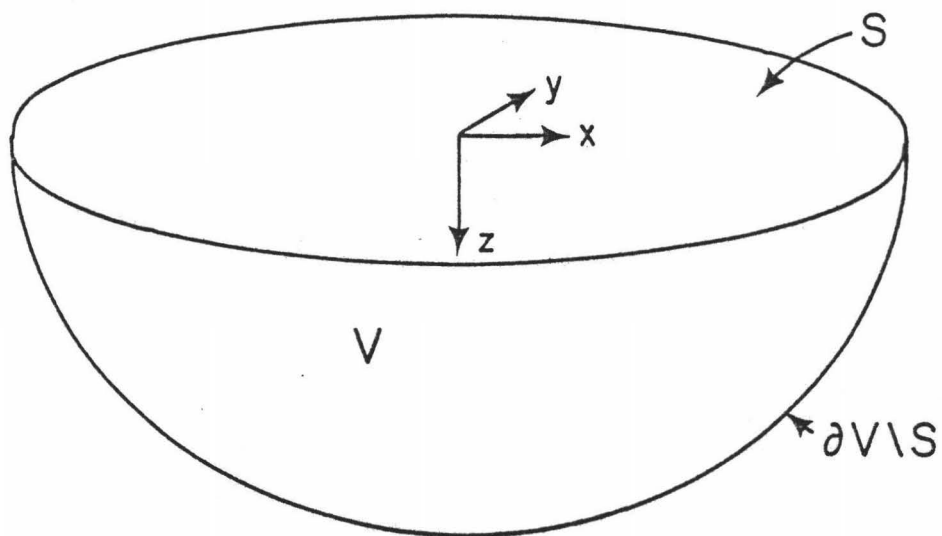


Figure 1: The integration volume  $V$  and surfaces  $S$  and  $\partial V \setminus S$ .



$$\partial_n G = (\partial_n |G|) e^{-i\omega\tau} - |G| e^{-i\omega\tau} i\omega (\partial_n \tau) \quad (6)$$

is small compared to the second and may be neglected. The Kirchhoff integral (5) may now be written in the form

$$\psi(\underline{r}_1, \omega) = -2 \int_S \psi(\underline{r}, \omega) |G| e^{-i\omega\tau} i\omega (\partial_n \tau) dS \quad (7)$$

in which

$$\partial_n \tau = \hat{n} \cdot \Delta \tau = \hat{n} \cdot \hat{t} / v_r = \cos \theta_r / v_r,$$

$\hat{t}$  is the tangent to the emerging ray,  $\theta_r$  is the angle of emergence (Figure 2), and  $v_r$  is the velocity at the receiver. The amplitude term ( $|G|$ ) is inversely proportional to the square root of the area of the ray tube that originates at the source and emerges at the surface.

Consider an annular ray tube that starts at depth  $z$  and emerges at horizontal surface offset  $\Delta$  (Figure 2). The area of the ray tube cross section at unit distance from the source is  $a_s = 2\pi \sin \theta_s d\theta_s$ , where  $\theta_s$  is the takeoff angle, and at the surface the area is  $a_r = 2\pi \Delta dl$ . The geometrical optics assumption is that energy flux is constant along a ray tube. Energy is proportional to the square of the amplitude so conservation of energy flux yields

$$\rho_s v_s a_s |G_s|^2 = \rho_r v_r a_r |G_r|^2 \quad (8)$$

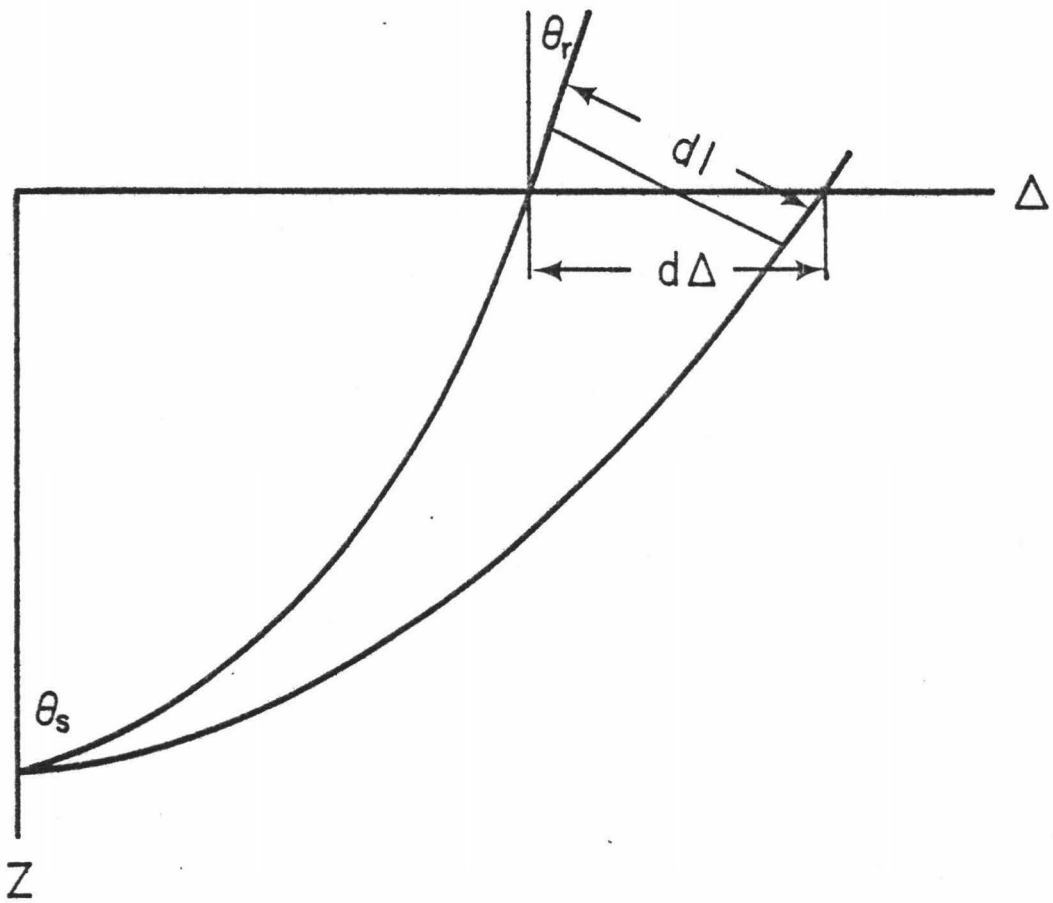


Figure 2: A ray tube originating at depth  $z$  and emerging at horizontal surface offset  $\Delta$ .  $\theta_s$  is the takeoff angle;  $\theta_r$  is the angle of emergence;  $dI$  is the width of the ray tube at the surface; and  $d\Delta$  is the intersection of the ray tube with the surface.

where  $v_s$ ,  $v_r$  and  $\rho_s$ ,  $\rho_r$  are the velocities and densities of the materials at the source and receiver, respectively. Near the source, the material can be regarded as homogeneous and the Greens function solution to the Helmholtz equation (1) is  $G_s = e^{i\omega r/c}/(-4\pi r)$ . Thus,  $|G_s|$  at unit distance is  $-1/4\pi$ . An expression must also be found for  $d\theta_s/dl$  in terms of parameters that are easily calculated. We use the ray parameter  $p$ , defined by  $p = \sin\theta(z)/v(z)$ , and surface offset  $\Delta$  to obtain  $d\theta_s/dl = v_s / (\cos\theta_r \cos\theta_s) dp/d\Delta$ . Substituting for these terms and solving for  $|G_r|$  we obtain

$$|G_r| = \frac{-1}{4\pi} \left\{ \rho_s v_s^2 \tan\theta_s \frac{dp}{d\Delta} / (\cos\theta_r \Delta \rho_r v_r) \right\}^{1/2}. \quad (9)$$

The Kirchhoff integral (equation 7) thus becomes

$$\psi(\underline{r}_1, \omega) = \frac{1}{2\pi} \int_S \left\{ \rho_s v_s^2 \cos\theta_r \tan\theta_s \frac{dp}{d\Delta} / (\Delta \rho_r v_r^3) \right\}^{1/2} i\omega e^{-i\omega\tau} \psi(\underline{r}, \omega) dS, \quad (10)$$

and transformation to the time domain yields

$$\psi(\underline{r}_1, t) = \frac{-1}{2\pi} \int_S \left\{ \rho_s v_s^2 \cos\theta_r \tan\theta_s \frac{dp}{d\Delta} / (\Delta \rho_r v_r^3) \right\}^{1/2} \partial_t \psi(\underline{r}, t+\tau) dS. \quad (11)$$

Equation (11) can be used to obtain the wavefield at any point in the subsurface for all times. In other words, we may migrate our source/receiver pairs down through the section obtaining a time section at any depth. By using only the time  $t=0$  arrivals from each source/receiver depth, we obtain the migrated depth section.

$$\psi(\underline{r}_1, 0) = \frac{-1}{2\pi} \int_S \{ \rho_s v_s^2 \cos^2 \theta_r \tan^3 \theta_s \frac{dp}{d\Delta} / (\Delta \rho_r v_r^3) \}^{1/2} \partial_t \psi(\underline{r}, \tau) dS. \quad (12)$$

For a subsurface point scatterer at depth  $z$ , the two-way travel time function  $\tau(\underline{r}, \underline{r}_1)$  is a three-dimensional migration surface and the coefficient of  $\partial_t \psi$  is the weighting factor for that surface.

Because the migration surfaces extend to infinity in both the horizontal direction and in time and our data do not, some practical limits must be placed upon the extent of the surfaces. The usual procedure is to restrict the horizontal extent of the surfaces to a distance known as the migration aperture. This procedure limits the number of traces that must be summed over for each migrated point but may also limit the accuracy of the migration. Greater accuracy may be obtained by increasing the width of the aperture, but the CPU time increases proportionately.

In most cases, the data collected in reflection seismology are assumed to be from two-dimensional geological structures. Assuming that the reflection line lies perpendicular to the strike of such a structure, the two-dimensional analog of equation (12) is obtained by integrating (12) over the independent variable (say,  $y$ ). Rather than perform this integration, we approximate the result by

$$\psi(x_1, z_1, 0) = \frac{1}{2\pi} \int_x \{ \rho_s v_s^2 \cos^3 \theta_r \tan^3 \theta_s \frac{dp}{d\Delta} / (\Delta \rho_r v_r^3) \}^{1/4} H^- \psi(x, 0, \tau) dx \quad (13)$$

where the operator  $H^-$  is defined by

$$\bar{H}^{-1}F(t) = \frac{1}{2\pi} \int_{-\infty}^{\infty} (i\omega)^{1/2} \left[ \int_{-\infty}^{\infty} F(t) e^{i\omega t} dt \right] e^{-i\omega t} d\omega. \quad (14)$$

The approximation errors all occur in the weighting factor where even a moderately large error will have little effect on the results. In the homogeneous case, (13) reduces to the formula given by Berkhout [1980] for two-dimensional data. For the more complicated case where the data are collected along a line oblique to the structure, an obliquity factor must be applied [French, 1975].

In equation (13) the function  $\tau$  now represents two-dimensional migration curves rather than the migration surfaces of equation (12). Determining the migration curves for a laterally varying velocity-depth function is a formidable problem as there is a distinct migration curve associated with each subsurface point and extensive ray tracing is necessary to determine the exact migration curves. If the velocity-depth function varies only with depth, however, the problem is significantly simplified. In this case, all of the points with a common depth have the same migration curve and the curves are easily determined. One approach is to approximate the migration curves with hyperbolas [French, 1974; 1975; Schneider, 1978] using root mean square (rms) velocities [Taner and Koehler, 1969] to the depths of the point scatterers. The rms approximation has been examined by several authors [e.g., Brown, 1969; Stoffa et al., 1982] for the determination of stacking velocities and has been found inadequate at large offsets.

Ray tracing is a more accurate method of determining the

migration curves but is not used because it requires an iterative scheme to determine the exact ray that originates at  $(0, z, t=0)$  and terminates at  $(\Delta, 0, \tau)$ . An alternate method that is nearly as accurate but less time consuming than the iterative method involves interpolation. The desired ray is interpolated from a group of several rays that have been traced at some constant ray parameter increment. The accuracy of this method depends on the surface spacing of rays used for the interpolation and the type of interpolation scheme used (e.g., linear, sinc, cubic spline). In Figure 3 we compare the rms and interpolation methods of determining the migration curve. Plotted are one-half of the exact curve, the rms curve, and the 10-ray interpolation curve for a point scatterer at the base of a 0.5-km layer of 2.5 km/s material overlain by 2.0 km of 1.5-km/s material. For this model, the rms migration curve is satisfactory at small offsets. Beyond 1.5-km offset, however, the error is greater than 10 ms. The 10-ray interpolated curve has less than 10 ms error out to 2.6 km; if we increase the number of rays used in the interpolation to 20, the error is further reduced to 2.3 ms at 3.0-km range. For all of the examples shown in this paper, a 20-ray interpolation was used.

By use of the ray approach the error is reduced to an interpolation error that can be made arbitrarily small by increasing the number of rays traced. This error is smallest at zero offset where the amplitude of the weighting factor is large, whereas at greater offsets, where the error is large, the weighting factor is

smaller. The extra accuracy obtained by using rays comes free, in a sense, because a knowledge of the ray path is required in order to incorporate the effects of the lateral velocity changes.

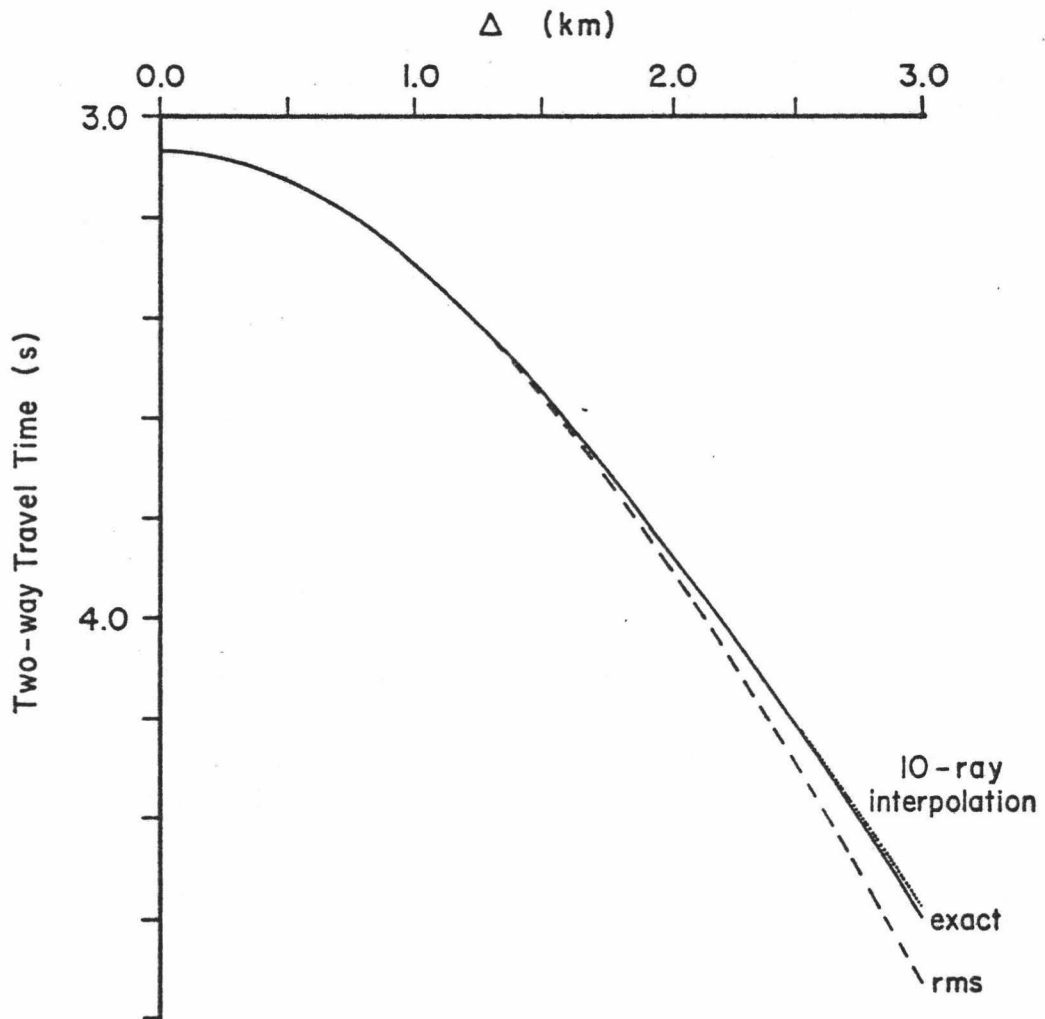


Figure 3: Approximations to the exact migration curve (solid line) for a point scatterer in a 2.5 km/s medium 0.5 km below 2.0 km of 1.5 km/s material. The rms curve (dashed) is more than 10ms in error beyond 1.5 km range. A three-point Lagrangian interpolation was used for the interpolation curve (dotted) and by increasing the number of rays used, the error may be made arbitrarily small.



## III. ACCOMODATING LATERAL VELOCITY CHANGES

As mentioned above, determining the exact migration curves for a velocity-depth function that varies laterally as well as with depth requires that rays be traced from each subsurface point to each receiver. To avoid this extensive ray trace, we calculate perturbations to the migration curves generated for a velocity function that varies only with depth.

We begin with a slowness-depth model  $d(x,z)$  which we write as the sum of a one-dimensional slowness-depth model  $a(z)$  (reference model) and a two-dimensional model of slowness perturbations  $b(x,z)$  (perturbation model) (Figure 4). The reference model is used to generate a set of rays emanating from several point scatterer depths and terminating at the surface (Figure 5). Two tables are generated: one of travel times and one of subsurface horizontal ray offsets. The travel time table  $T(p,z)$  is a function of ray parameter,  $p$ , and scatterer depth,  $z$ . The table of subsurface horizontal ray offsets  $\xi(\zeta,p,z)$  has entries for ray depth,  $\zeta$ , ray parameter,  $p$ , and scatterer depth,  $z$ . Because our data traces are evenly spaced along the surface and, in general, the model depth spacing is coarser than the depth spacing of the migrated section, we interpolate to find the travel times and subsurface horizontal ray offsets of the rays that have starting depths  $z_j$  and emerge at surface offsets  $\Delta_i$  (Figure 6). Interpolation of the tables for these values results in new tables  $T(\Delta,z)$  and  $\xi(\zeta,\Delta,z)$ . The table  $T(\Delta,z)$  defines the migration curves

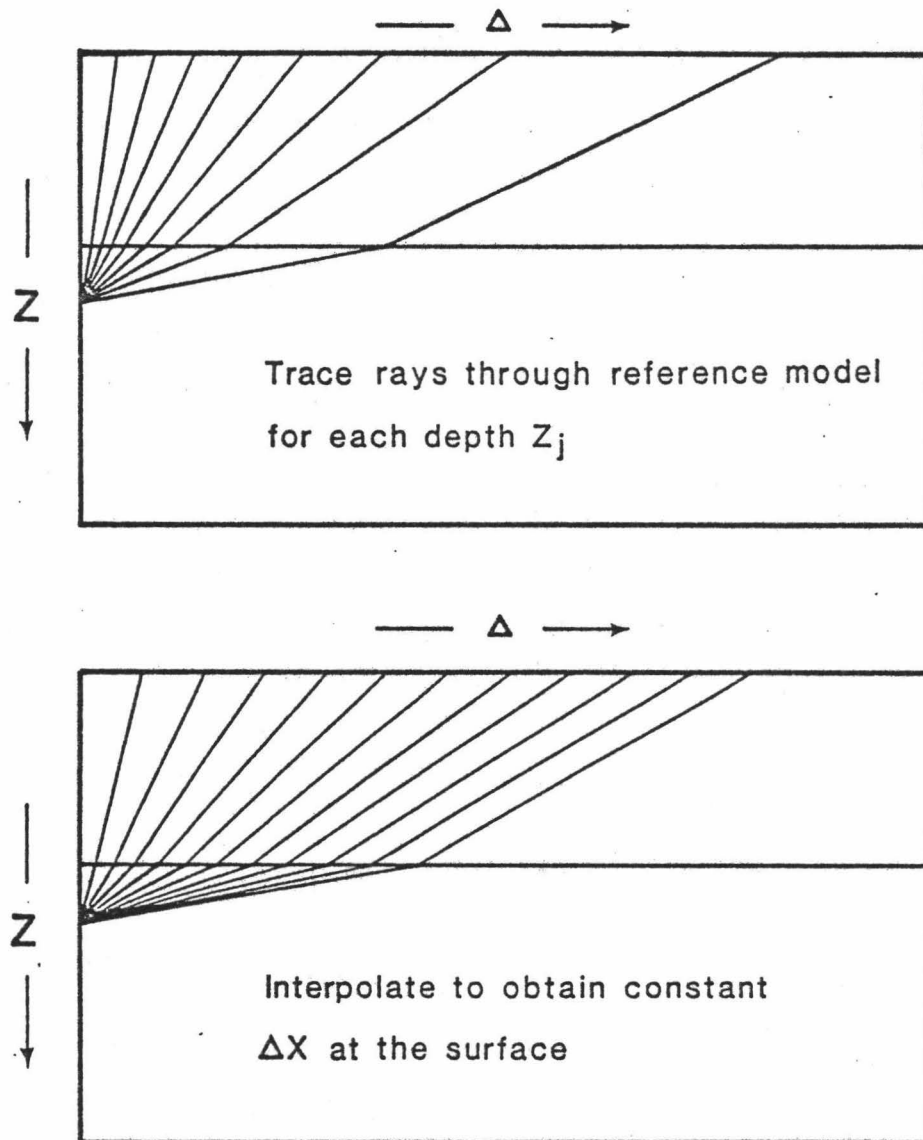


Figure 5: Rays are traced through the reference model at a constant ray parameter increment. Then, interpolation is used to obtain the rays which intersect the surface at a constant surface offset increment.

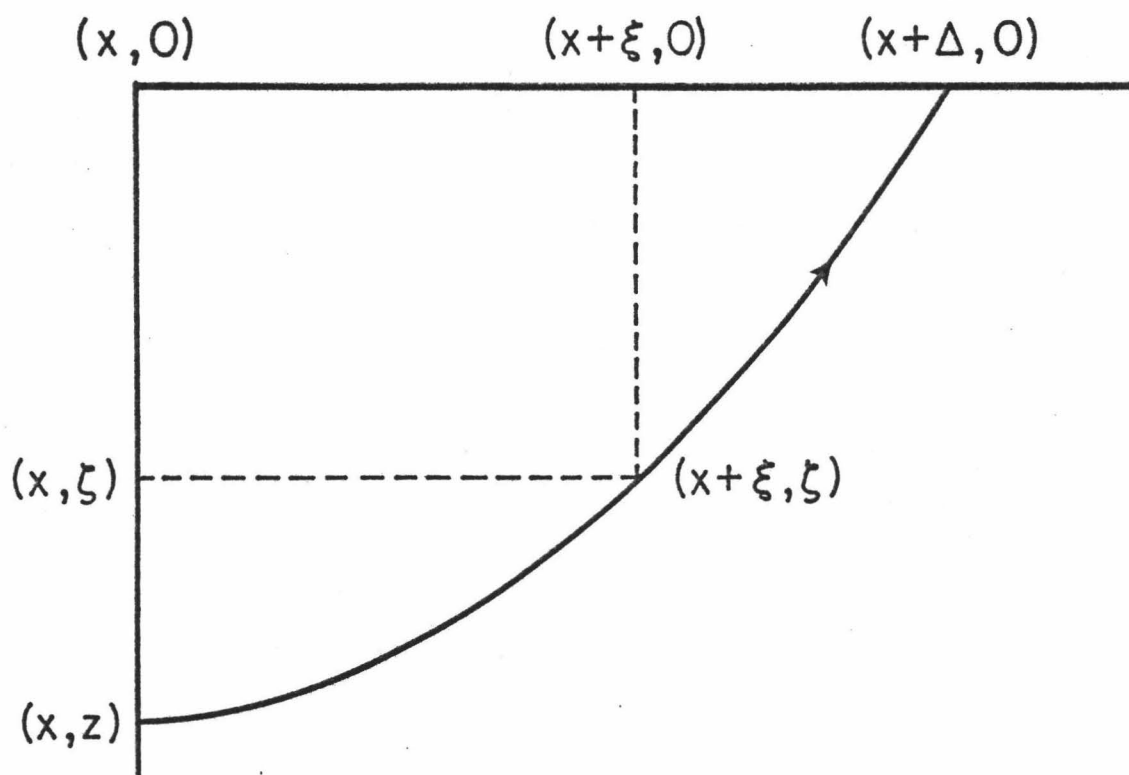


Figure 6: A ray from a depth point  $(x, z)$  to a source/receiver point  $(x+\Delta, 0)$ . A point on the ray has coordinates  $(x+\xi, \zeta)$  where  $0 \leq \xi \leq \Delta$  and  $0 \leq \zeta \leq z$ .

that would be used in conventional migration and the table  $\xi(\zeta, \Delta, z)$  contains the subsurface positions of the rays.

We now assume that the raypaths just determined do not deviate substantially from the raypaths that would have been drawn through the original model  $d(x, z)$ . Fermat's principle, which states that the raypath between any two points in a medium is that for which the travel time is stationary, then allows us to calculate approximations to the exact migration curves by calculating the travel times of the reference model rays in the original model  $d(x, z)$ . The travel times through the reference model have been determined above, but the effect of the perturbation model must still be determined. Assuming that the ray path deviation due to the slowness function  $b(x, z)$  is small, the travel time difference  $T_0(x, \Delta, z)$  caused by the slowness perturbations  $b(x, z)$  can be approximated by integrating over the unperturbed ray path (Figure 7a)

$$T_0(x, \Delta, z) = \int b(x + \xi, \zeta) ds. \quad (15)$$

The travel-time perturbations,  $T_0(x, \Delta, z)$ , are then added to the migration curve  $T(\Delta, z)$  computed from the reference model to obtain an approximation to the exact migration curve for the point  $(x, z)$  (Figure 7b)

$$\tau(x, \Delta, z) = T(\Delta, z) + T_0(x, \Delta, z). \quad (16)$$

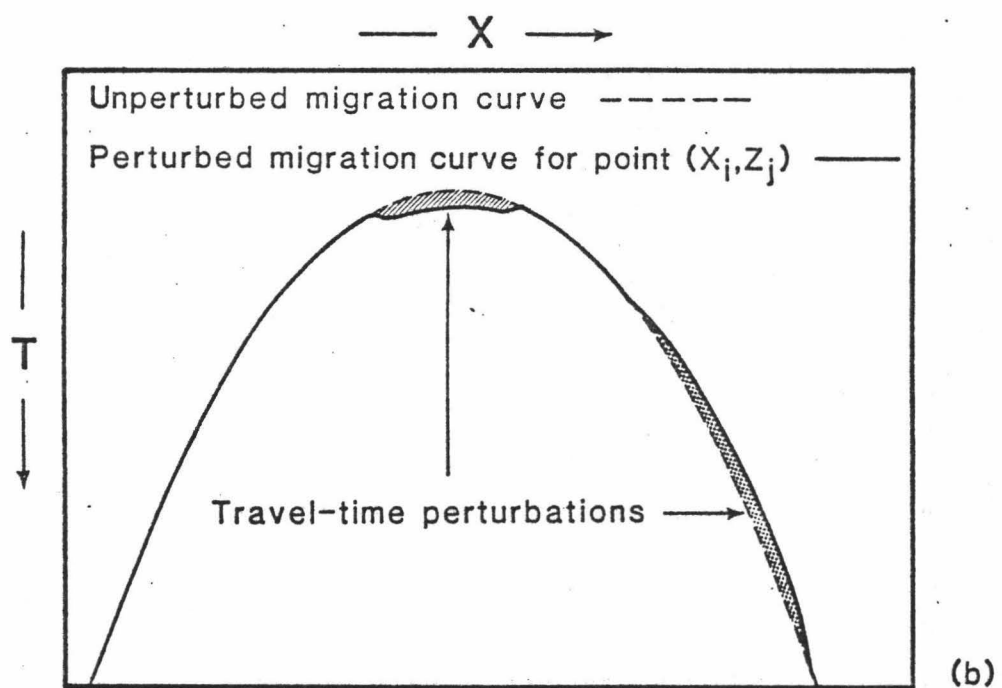
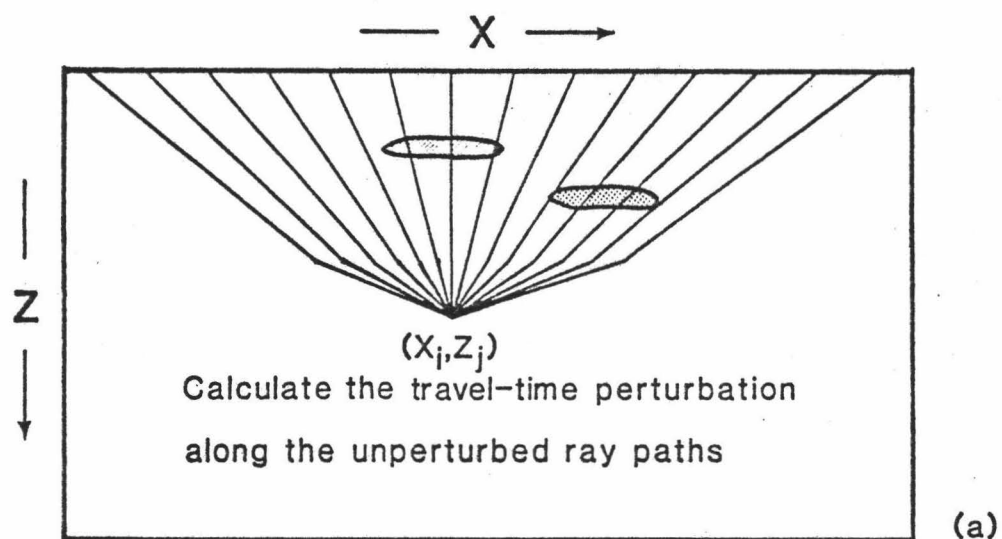


Figure 7: (a) Travel-time corrections to the migration curve are determined by using the travel paths of the unperturbed rays in the slowness perturbation model. (b) The travel-time differences are added to the usual migration curves to produce an approximation to the exact migration curves.

Computation of the travel time perturbations can take a significant amount of computer time as the perturbations must be calculated for the migration curves of all subsurface points in the migrated section. Therefore, the depth sample spacing of the slowness model has the largest influence over the computer time required. As the complexity of the model increases, more model depth points are required, increasing the computation time necessary. For the examples shown below, there is one model depth point for every five depth points in the migrated section. In each migrated trace there are 296 depth points and each section contains 200 traces. Conventional Kirchhoff migrations (i.e., ones that do not account for lateral velocity variations) required about 3.5 min of CPU time on an HARRIS 800 computer that has a Whetstone number of 1470. Including the velocity perturbations increased the amount of CPU time necessary to about 40 min, a significant increase but still well below the estimated CPU time required to compute the exact migration curves by using two-dimensional ray tracing.

## IV. EXAMPLES

Synthetic reflection profiles of two-dimensional structures were provided by Amoco Production Company for the purpose of testing and demonstrating the theory presented above. A finite difference algorithm was used to generate the synthetic sections.

The first example (Figure 8a) consists of a surface layer in which there are two lenses, one low-velocity lens and one high-velocity lens, a second layer with a velocity fifty percent higher than that of the surface layer, and an anticlinal basement layer. The finite-difference synthetic data for this section are shown in Figure 8b. Velocity pull-ups and pull-downs can be seen on the lower edges of the lenses, the horizontal interface, and the anticline. The upper lens has a lower velocity than the surrounding material and causes a pull-down, whereas the lower lens is of a higher velocity and causes a pull-up. The first large pulse at the upper edge of the upper lens is negative (unshaded), corresponding to the negative acoustic impedance contrast at the interface whereas the lower edge has a positive motion due to the positive acoustic impedance contrast. The opposite is true for the lower lens.

A conventional Kirchhoff migration was performed on the section in Figure 8b to obtain the section shown in Figure 8c. The diffractions from the edges of the lenses have been properly collapsed but the effects of the velocity differences remain. The low-velocity lens is too thick, the high-velocity lens is too thin, and the

pull-ups and pull-downs on the horizontal interface and anticline have not been corrected. When the horizontal velocity variations are accounted for, however, these defects are corrected (Figure 8d). Not only have the diffraction patterns from the edges of the lenses been collapsed, but also the lenses have been migrated to their proper thicknesses and the velocity pull-ups and pull-downs have been corrected.

For the second example an asymmetrical syncline has been added to the horizontal layer of the previous example. The material filling the syncline has the same velocity as the surface layer but a lower density so there is a negative acoustic impedance contrast along the horizontal interface above the syncline (Figure 9a). Synthetic data for this section are shown in Figure 9b. The familiar 'bow tie' pattern is caused by the syncline. The anticlinal horizon has been pulled down by the low velocity of the material in the syncline but there is a slight bow tie pattern at this interface, also.

Figure 9c shows a conventional Kirchhoff migration of these data. As in Figure 8c, the velocity pull-ups and pull-downs have not been corrected. The thicknesses of the lenses are not correct, the horizontal interface still deviates from the horizontal, and the syncline and anticline appear severely distorted. Proper interpretation of this migrated section would be difficult.

When the lateral velocity variations are included in the migration (Figure 9d), many of these problems are resolved; lens thicknesses are correct and the horizontal layer shows no velocity



pull-ups or pull-downs. Some energy is missing from the edges of the syncline, however, and the amplitudes along the anticline are not consistent. These problems arise because the velocity contrast across the syncline interface is large enough to change the raypaths significantly, thus violating our assumption of small raypath perturbations. Despite the violation of our assumptions and the resulting inaccuracies, a significant improvement over the conventional Kirchoff migration has been obtained.

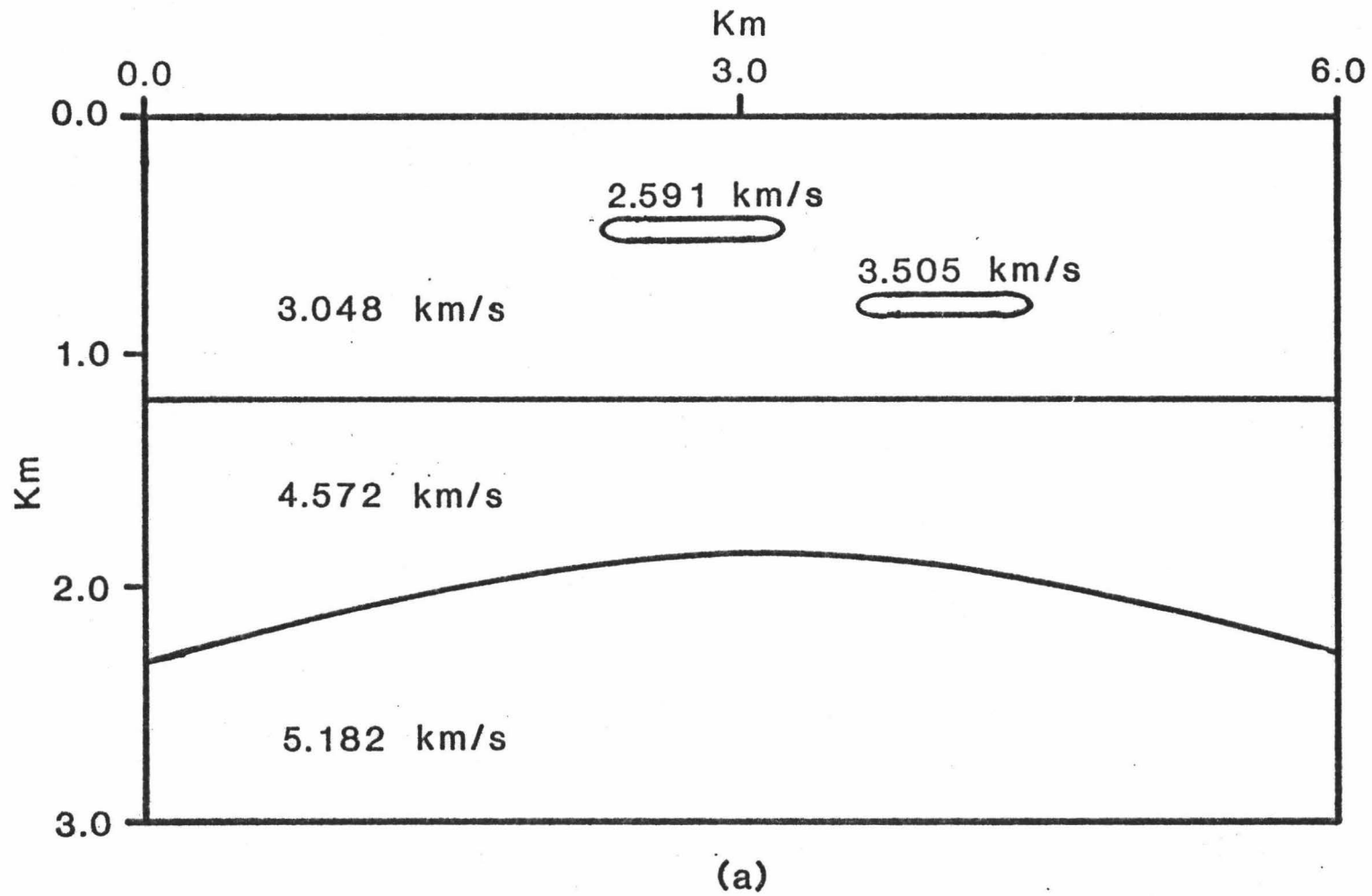
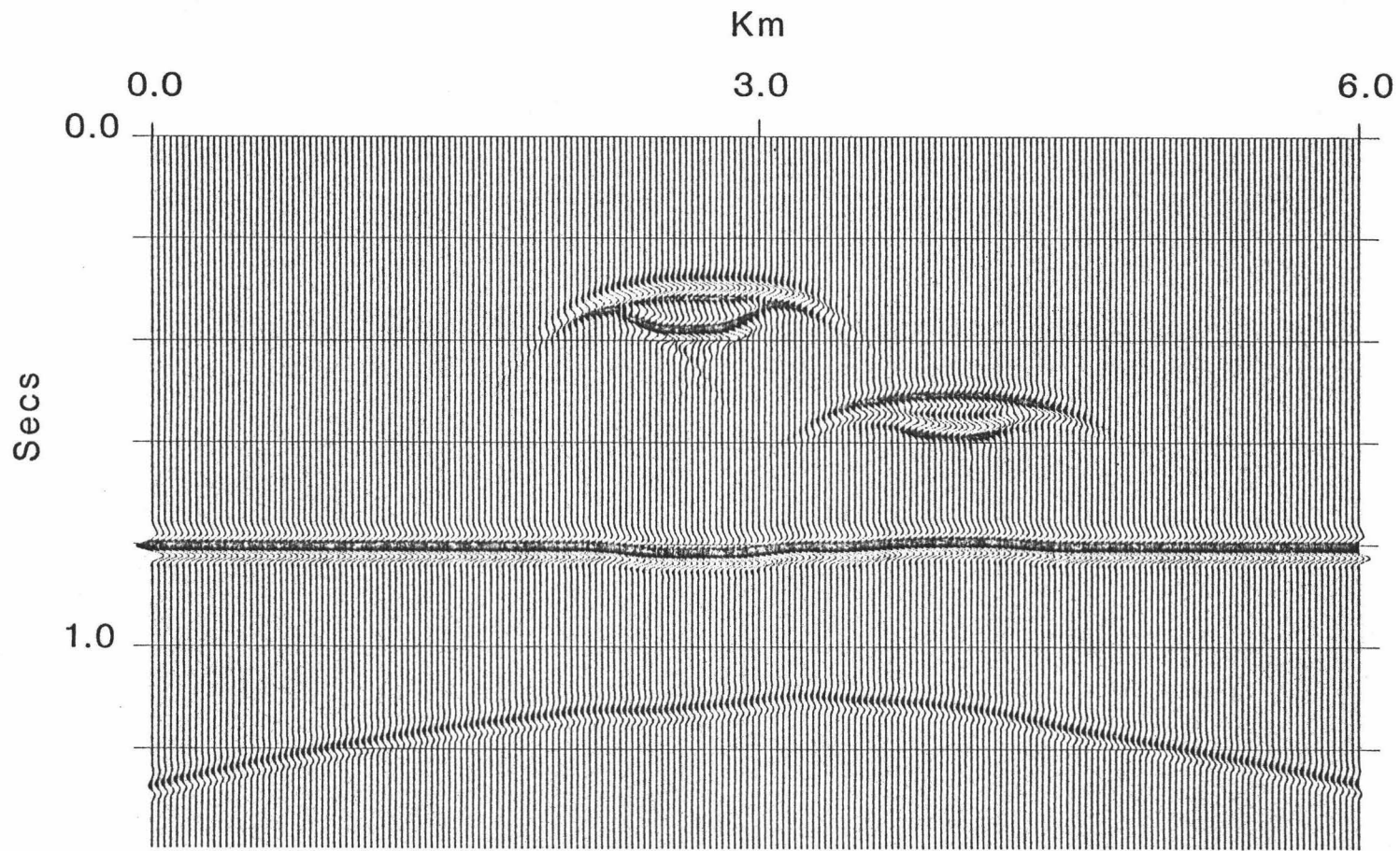


Figure 8: (a) The velocity-depth model used to generate the finite difference synthetic record section.



(b)

Figure 8: (b) Synthetic data for the model in (a). Velocity pull-ups and pull-downs are apparent along the horizontal and anticlinal interfaces.

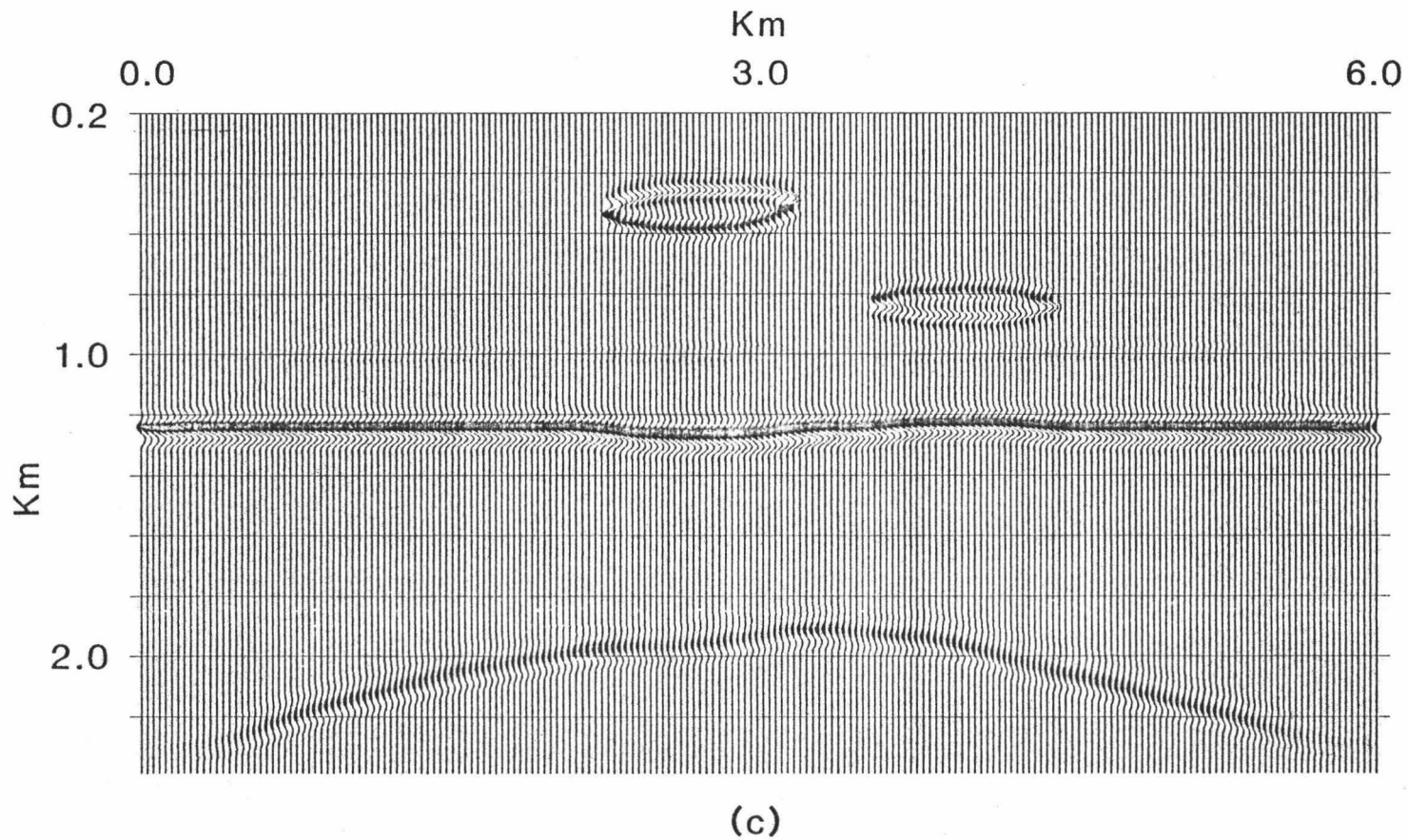


Figure 8: (c) A conventional (no horizontal velocity variations) Kirchhoff migration of the data in (b). Velocity pull-ups and pull-downs remain.

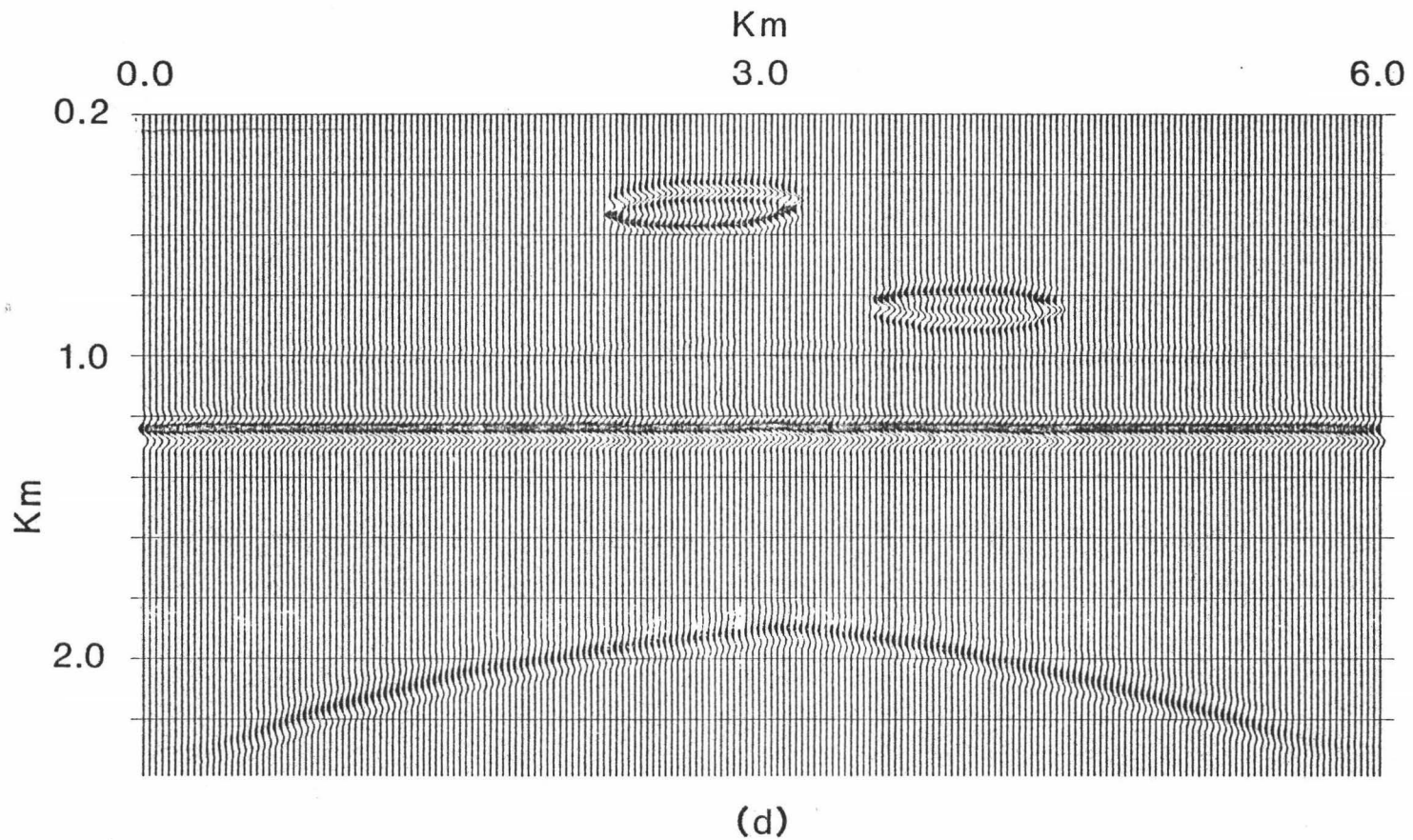


Figure 8: (d) A Kirchhoff migration of (b) accounting for the horizontal velocity variations by using the method described in this dissertation. The effects of the lenses have been removed.

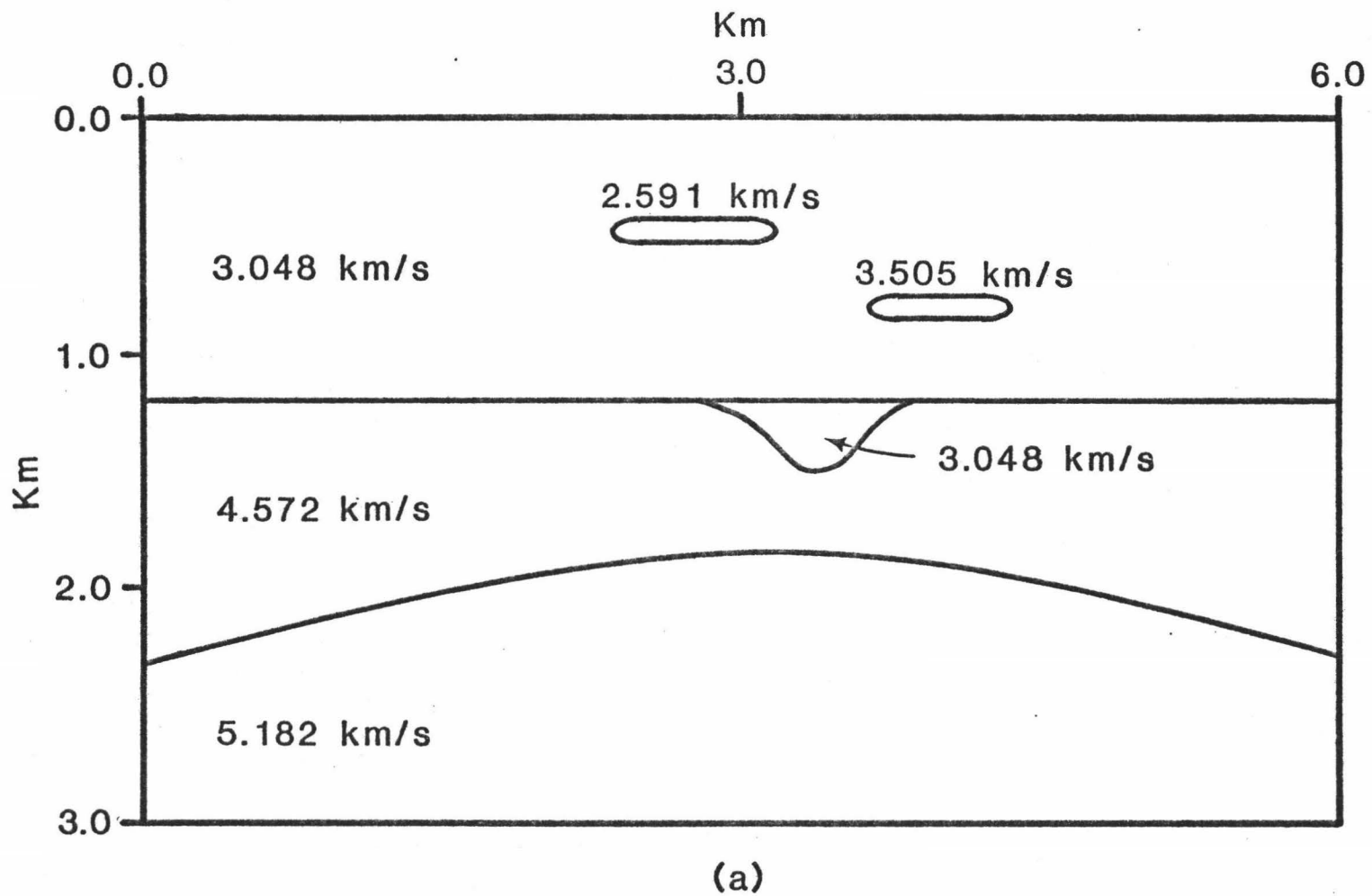
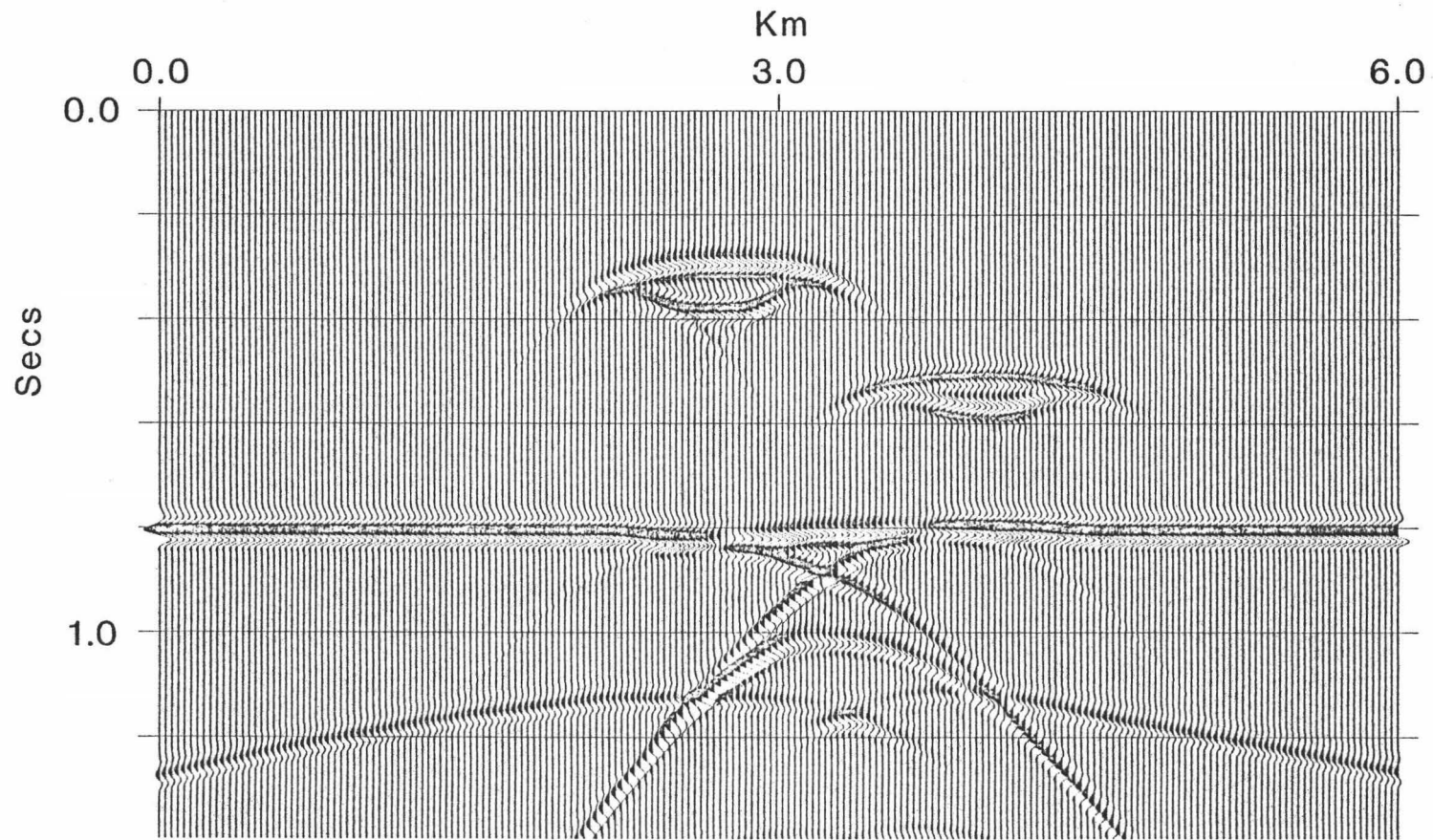


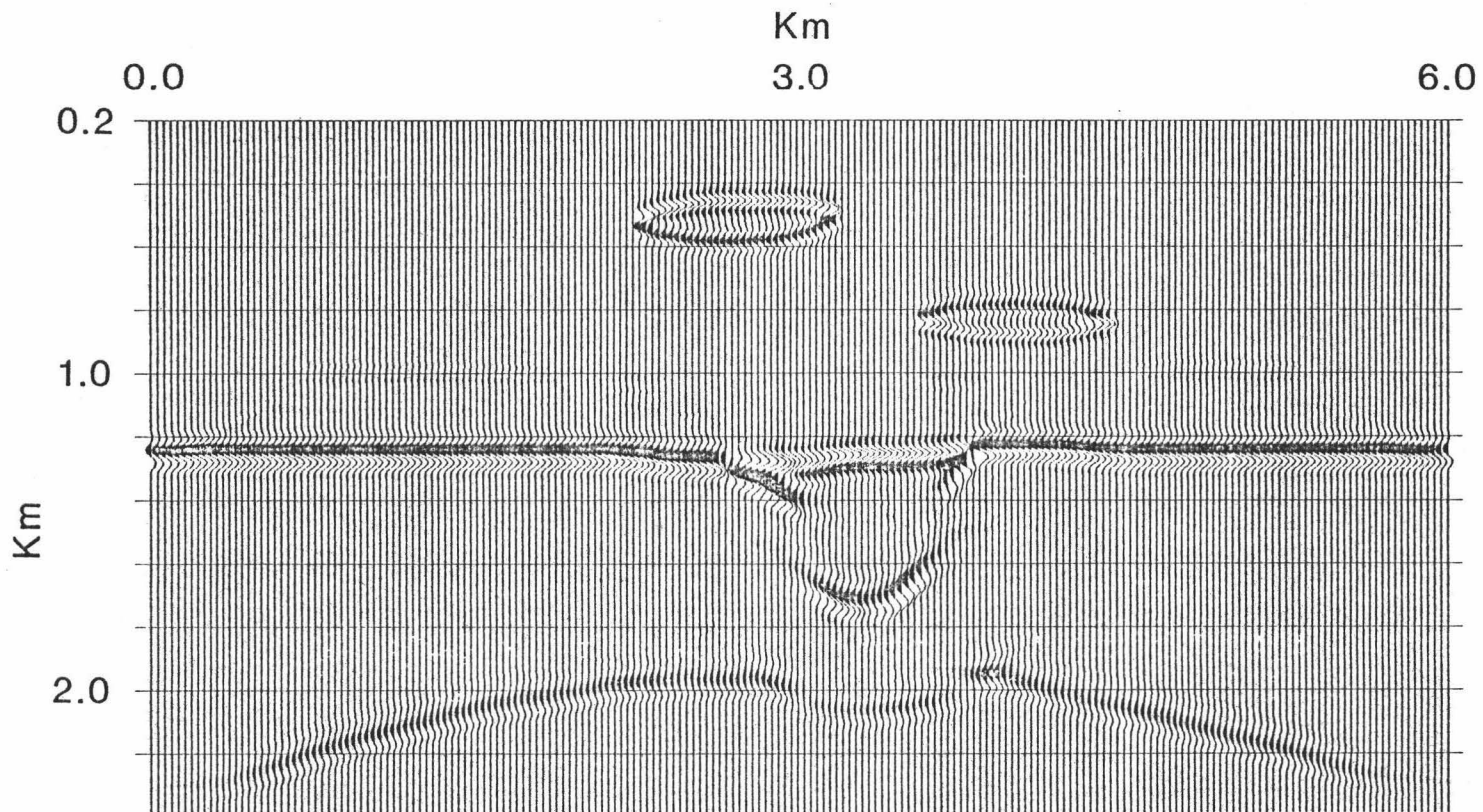
Figure 9: (a) The velocity-depth model used to generate the finite difference synthetic record section.



(b)

Figure 9: (b) A Synthetic record section for the model in (a). In addition to the velocity pull-ups and pull-downs along the horizontal and anticlinal interfaces there is now a bow-tie pattern due to the syncline.

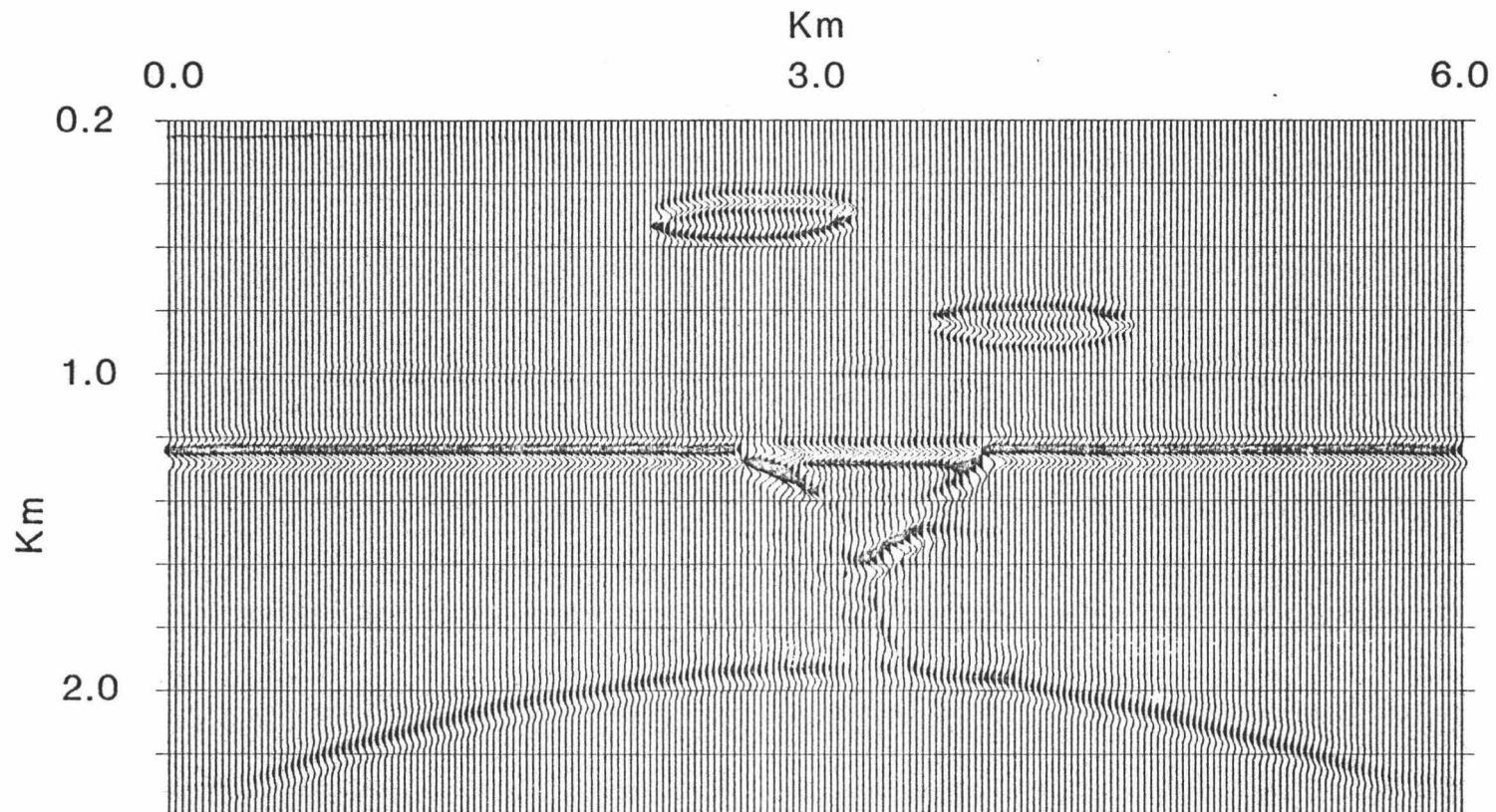




(c)

Figure 9: (c) A conventional (no horizontal velocity variations) Kirchhoff migration of the data in (b). The velocity pull-ups and pull-downs remain and the syncline and anticline are severely distorted.





(d)

Figure 9: (d) A Kirchhoff migration of (b) accounting for the horizontal velocity variations by using the method described in this dissertation. Although some energy is missing, the syncline and anticline have been restored to their correct shapes.

## V. MODELING: THE FORWARD PROBLEM

Forward modeling of zero-offset reflection sections has been applied to many areas of research. In addition to their use as a tool in the interpretation of analog reflection profiles, modeling programs have been used extensively to study the reflection and diffraction processes [Hilterman, 1970; 1975; Trorey, 1970; Berryhill, 1977].

The modeling techniques presented in the literature have nearly all been based on the Kirchhoff integral solution to the wave equation and nearly all have assumed a constant velocity medium [Hilterman, 1970; 1975; 1982; Trorey, 1970]. Mitzner [1967] wrote the Kirchhoff surface integral for a constant velocity medium as an integral over the solid angle subtended at the shot point by the intersection of the wavefront with the reflector surface. Hilterman [1970] used this form of the integral to model the response of three-dimensional surfaces. In order to simplify the computation of the solid angles, reflector surfaces were taken to be peicewise cylindrical or planar. With all such methods, as the reflector surface is made more complex, the number of planar strips required to model it increases along with the computation time required. In addition, if a velocity discontinuity is placed between the integration surface and the receiver point, the solid angle computations require more time.

In a later paper, Hilterman [1975] showed that for a constant velocity model with no source/receiver offset, the Kirchhoff integral could be written as a convolution of the time derivative of the solid

angle subtended at the shotpoint by the intersection of the wavefront with the surface and the derivative of the source wavelet. Curvature and diffraction effects were computed to account for the amplitude changes expected for these features, but lateral changes in the reflection coefficient were ignored.

Trorey [1970] also assumed a constant velocity medium and was able to write the solution to the problem of reflection from a half-plane in closed form as the sum of the reflection from an infinite plane and a diffraction from the edge of the plane. In his method, the input depth section is again piecewise planar. The reflection coefficient was assumed to be constant over the integration surface. This procedure was extended by Hilterman [1982] to handle three-dimensional surfaces consisting of contiguous triangular facets.

By integrating over source/receiver wavefronts rather than reflector surfaces, Frazer and Carter [1982] were able to accommodate both a velocity that varied with depth and continuous variations in subsurface reflectance. With their method the time of computation was relatively long, but was independent of the number and nature of subsurface reflectors.

Equation (11) was derived for extrapolation of the wavefield backward in time. In the forward application a positive phase is used in the expression for  $G$ ,  $G=|G|e^{i\omega\tau}$  and the integration volume  $V$  is redefined to be the upper half space in Figure 1. The resulting equation for forward propagation is then

$$\psi(\underline{r}_1, t) = \frac{-1}{2\pi} \int_S \{ \rho_s v_s^2 \cos \theta_r \tan \theta_s \frac{d\rho}{d\Delta} / (\Delta \rho_r v_r^3) \}^{1/2} \partial_t \psi(\underline{r}, t-\tau) dS \quad (17)$$

Equation (17) may be used to propagate the wave field on  $S$  to any point above the surface  $S$ . For the forward modeling application we wish to know the field at  $z_1=0$  due to all surfaces  $S$  in the input model. The input model consists of a depth section. At the interfaces,  $\psi(\underline{r}, t-\tau)$  is assigned the value of the reflectivity, and at all other points  $\psi$  is zero. Summing the contributions of the  $S$  integrations for every input model depth gives a single synthetic trace;

$$\psi(x_1, y_1, 0, t) = W(t) * \frac{-1}{2\pi} \partial_t \int_z \int_S \{ \rho_s v_s^2 \cos \theta_r \tan \theta_s \frac{d\rho}{d\Delta} / (\Delta \rho_r v_r^3) \}^{1/2} \psi(\underline{r}, t-\tau) dS dz \quad (18)$$

and in the two-dimensional case,

$$\psi(x_1, 0, t) = W(t) * \frac{1}{2\pi} \int_z \int_x \{ \rho_s v_s^2 \cos^3 \theta_r \tan \theta_s \frac{d\rho}{d\Delta} / (\Delta \rho_r v_r^3) \}^{1/4} \psi(x, z, t-\tau) dx dz \quad (19)$$

where  $W(t)$  is a source wavelet and  $*$  denotes convolution. Examining (18) and (19) closely, we see that the input data  $\psi(\underline{r}, t-\tau)$  are defined only at time  $t-\tau=0$  for all depths which restricts the integrals to times  $t=\tau$ . To obtain the value of the synthetic trace at time  $t$  then, equations (18) and (19) become integrals over the wavefronts emanating from the point  $\psi(x_1, y_1, 0)$  [Frazer and Carter, 1982]. Although

integrating over the wavefronts makes this method independent of the model complexity, it is an inefficient process since at most of the points along the wavefront,  $\psi(\underline{r}, 0)$  will be zero. If we could avoid summing the zero contributions, the process could be made more practical.

Consider a single subsurface point scatterer beneath a line of source/receiver pairs. The synthetic reflection section generated by use of (19) gives a curve that is analogous to a migration curve (Figure 10). By distributing the energy of the point scatterer over the migration curve, the same synthetic section could have been generated. For the modeling application, we shall refer to this curve as the diffraction curve. As Trorey [1970] points out and Gardner et al. [1974] demonstrate, all reflections are ensembles of diffractions; thus, if we compute the diffraction curve at each point in the time section for the corresponding point in the depth model, the ensemble of these curves will be a synthetic section. Because the time points do not correspond exactly to the samples in the depth model, linear interpolation is used to determine the reflectivity value. To avoid excluding points in the depth model, the sample time interval  $\Delta t$  is made small compared to the sample depth interval ( $\Delta t \ll \Delta z/v$ ).

The assumption implicit here is that every subsurface point behaves as a point scatterer; because every subsurface point is independent of the others, each point may be assigned a different reflectivity, thus allowing continuous changes in reflectivity throughout the model. The contribution to the integral of the zeros

along the wavefronts is avoided because the zeros in the model may be ignored when distributing the energy over the diffraction curves. This makes the computation time dependent upon the complexity of the input model but the upper limit is the time required to integrate over the wavefronts.

The method outlined above is fundamentally the same as that used for Kirchhoff migration, the only difference being that instead of summing over the migration curves in the time section to produce a migrated depth section, the energy in the depth section is distributed over the diffraction curves to obtain a synthetic time section. Because the migration and diffraction curves are analogous, lateral velocity variations may be accommodated in the same way that they were for migration.

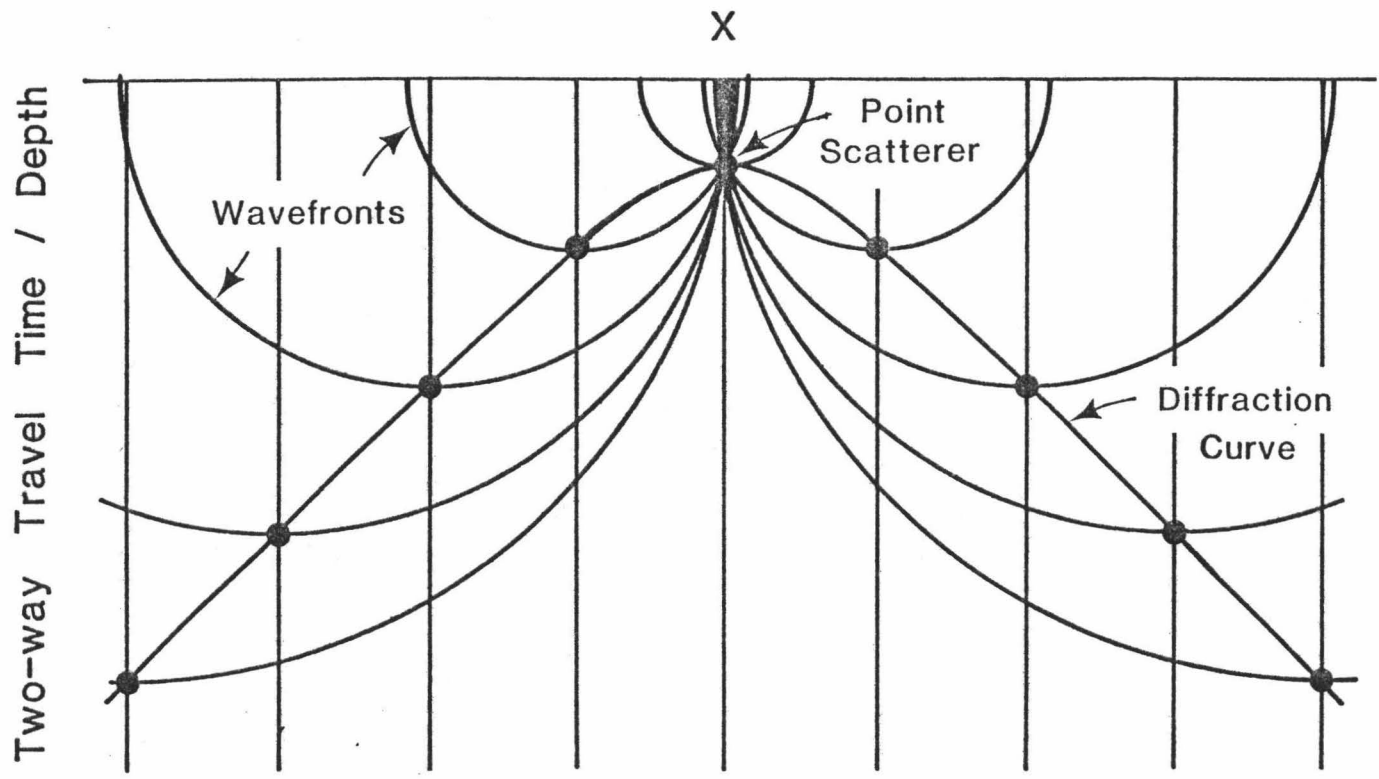


Figure 10: The synthetic section obtained from equation (19) for a point scatterer is analogous to a migration curve.

## VI. FORWARD MODELING EXAMPLE

The ideal test of a forward modeling program is to compare a data set from a well-known geologic structure to the synthetic section produced by the program. Unfortunately, the velocity control of most geologic sections is not adequate for our purposes, and so we utilize a physical model data set for our comparison. The model data are of a reef and were collected by employees of the Mobil Exploration Services Center using a modeling apparatus at Southern Methodist University. The physical models' scaled dimensions and velocities are shown in Figure 11a and the data set collected is displayed in Figure 11b. Although the data are somewhat noisy, there are several features which make this section a good one for emphasizing the strengths and weaknesses of a synthetic modeling method. First, note that the energy returning from the horizons at the edges of the reef has been displaced and that diffractions occur where these horizons terminate. Modeling these features is the most basic requirement of any synthetic program. The second dominant feature of this data set is the velocity pullup associated with the main body of the reef and the superimposed pulldown from the 30% porosity reef cap. These features are most easily observed in Figure 11b on the reflections from the bottom of the model. Another feature of interest in this data set is the presence of multiples. The surface multiple from the top of the reef appears at 1.4 s and again at 2.1 s. Interbed multiples from the reef cap dominate the center of the section and the coherent noise beneath



the reef edges between 1.8 and 2.3 s is probably due to interbed multiples from the edges of the reef. The steeply dipping arrival entering from the right edge of the section is a reflection from the edge of the model and should be ignored.

Figures 11c and d are a conventional Kirchhoff synthetic section (made without including lateral velocity variations), and a Kirchhoff synthetic section that includes lateral velocity variations by using the method described in chapter III, respectively. Both versions of the synthetic program have modeled the diffractions and horizon displacements quite well. In Figure 11d the exact location of the returning energy is somewhat closer to the model data due to the inclusion of the lateral velocity variations. The most obvious difference between the two synthetics is in their ability to model the velocity pullups and pulldowns. As expected, these features are correctly modeled in Figure 11d where the lateral velocity variations are accommodated. To obtain a fit to the data using the conventional Kirchhoff modeling routine, we would have to distort the horizons at the bottom of the reef cap, at the lower edge of the reef, and at the bottom of the model. Neither synthetic models the multiples that occur throughout the data section.

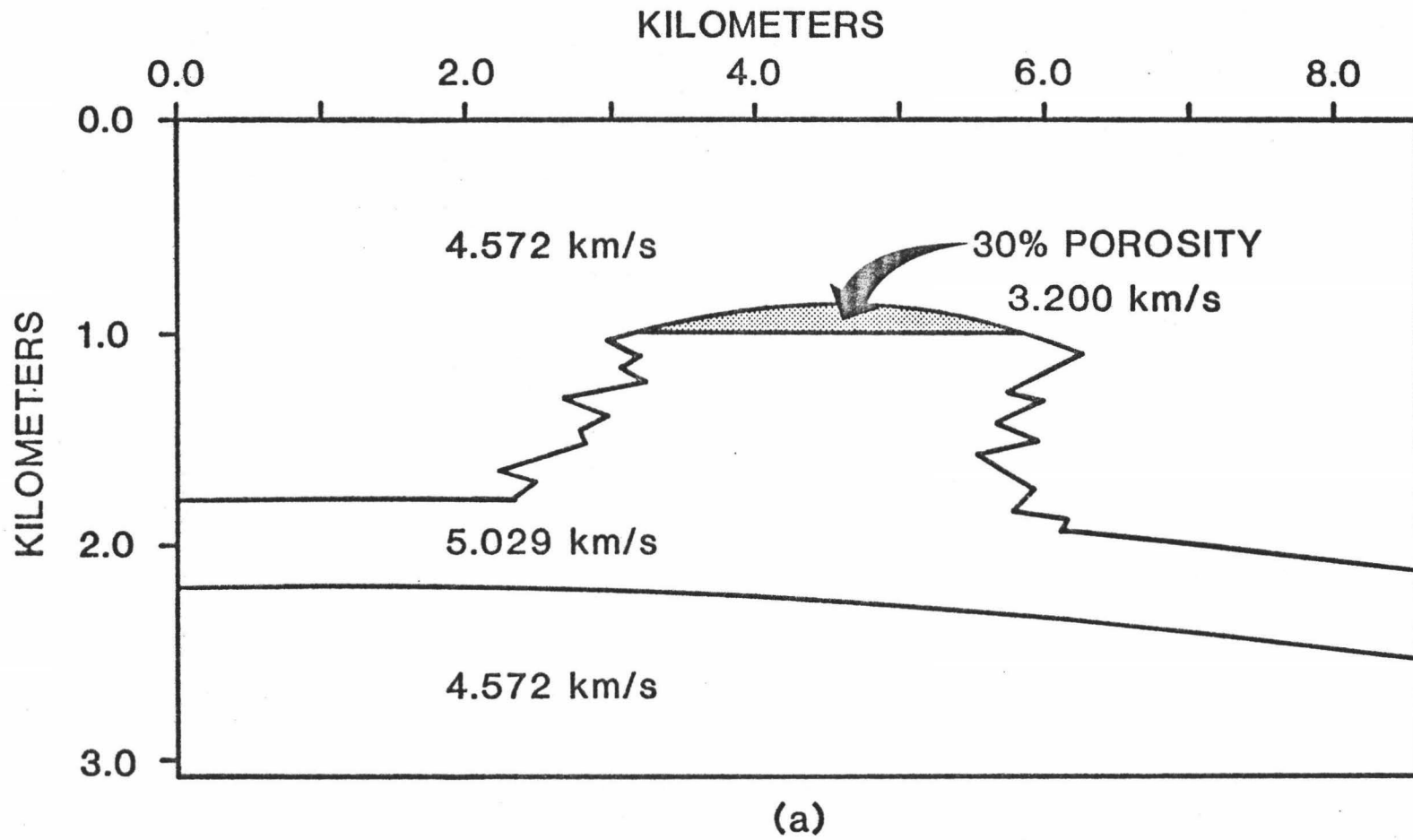
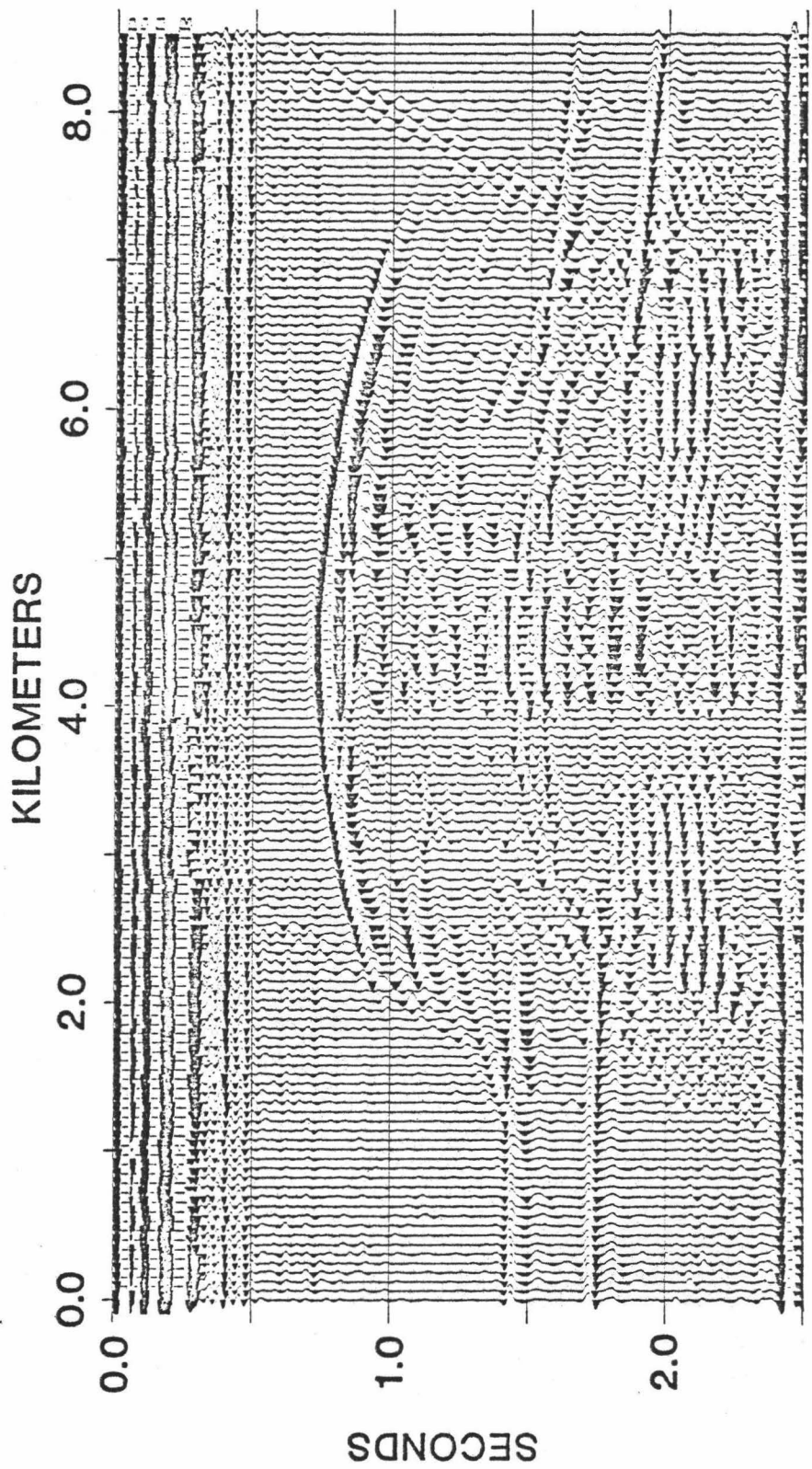
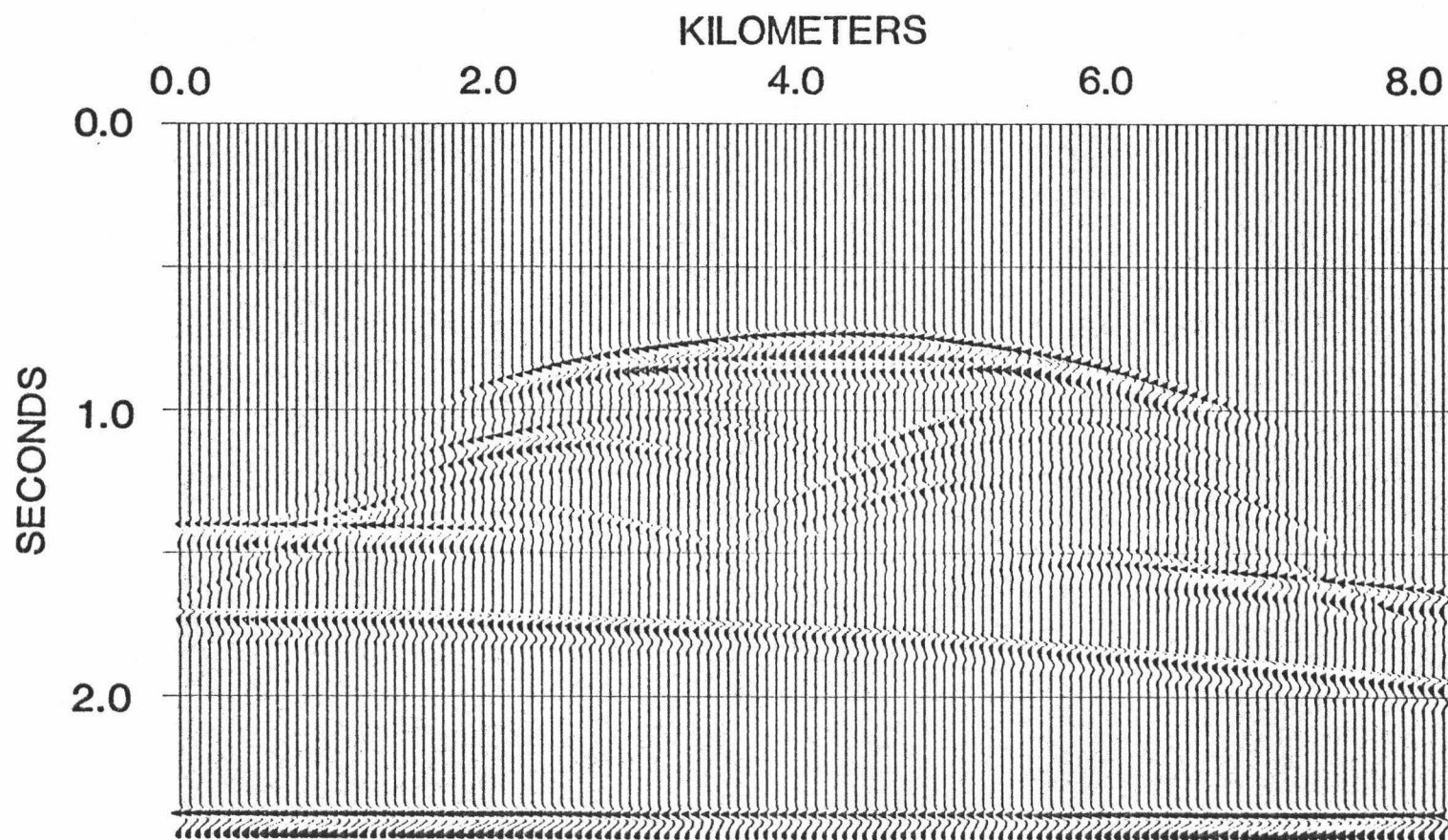


Figure 11: (a) Scaled velocity-depth function of the physical model.



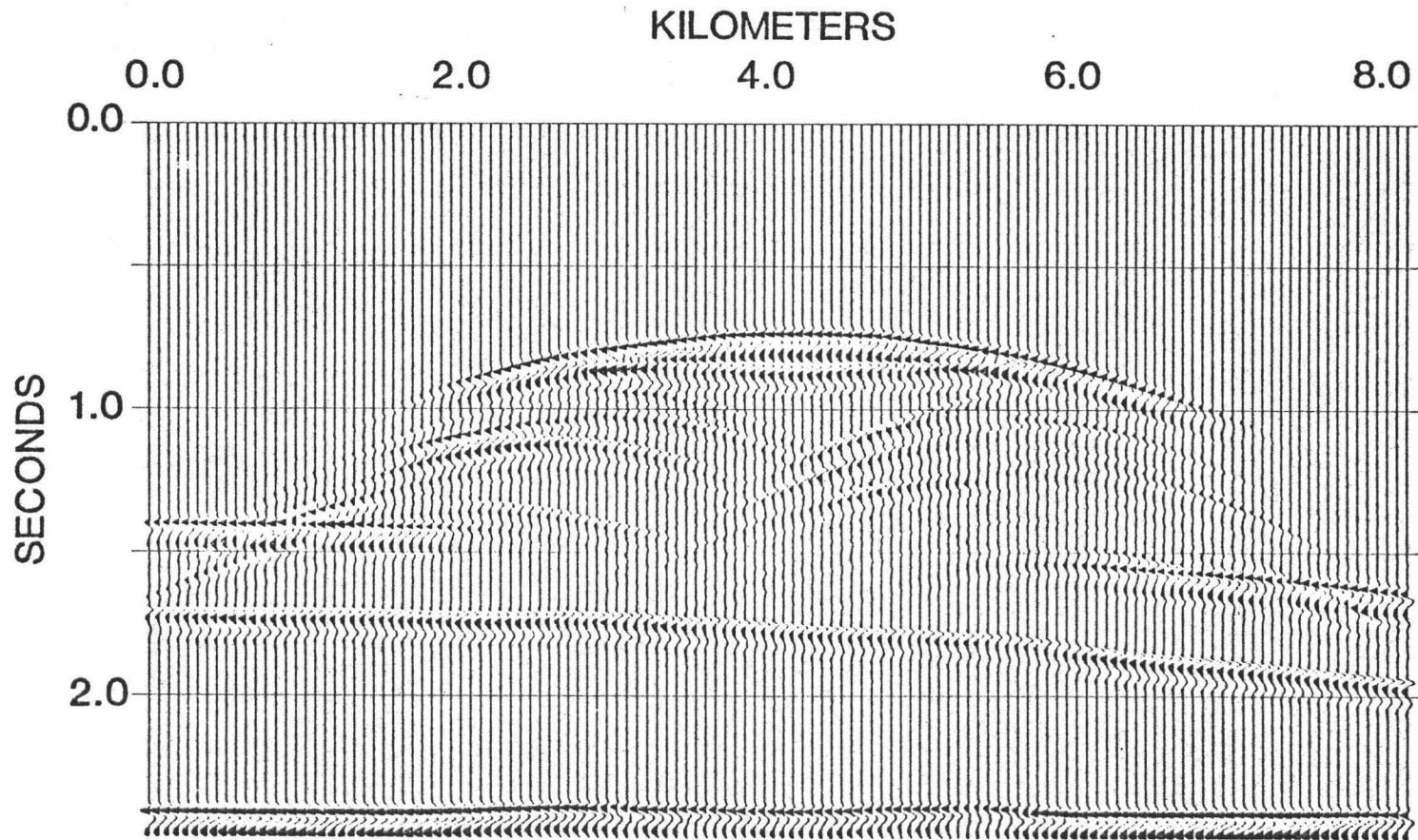
(b)

Figure 11: (b) Physical model data (courtesy of Mobil).



(c)

Figure 11: (c) Conventional Kirchhoff synthetic of the model in (a).



(d)

Figure 11: (d) Kirchhoff synthetic of (a) in which lateral velocity variations are accommodated.

## VII. CONCLUSIONS

A new method of accomodating lateral velocity variations in Kirchhoff migration has been presented that avoids the extensive ray tracing required to determine the exact migration curves for a model that varies laterally as well as with depth. The major assumption of this method is that the raypaths for the reference model do not deviate substantially from the raypaths that would be drawn through the original model. Fermat's principle then assures us that the travel times of these reference rays in the original model are first order approximations to the exact travel times. Even when the assumption of "small" lateral velocity changes is violated, significant improvements over conventional Kirchhoff migration may be obtained with this method.

We summarize the method as follows. First, an estimate is made of the slowness-depth function to be migrated. This model is written as the sum of a reference model that varies only with depth and a perturbation model that varies both laterally and with depth. The reference model is used to generate a table of travel times which define the migration curves as in conventional Kirchhoff migration, and a table of subsurface ray positions. This latter table is then used to determine the additional (positive or negative) travel time of the rays through the perturbation model for each subsurface point. The exact migration curves are approximated by adding these additional travel times to the migration curves determined for the reference

model.

The method can also be applied to forward modeling problems. The resulting synthetic sections can be used to improve interpretation of analog records and as a teaching tool for reflection seismology.

The computer time required to accommodate the lateral velocity variations is roughly an order of magnitude larger than that needed for conventional Kirchhoff migration or modeling.

## REFERENCES

- Berkhout, A.J., Seismic Migration, 339pp., Elsevier, Amsterdam, 1980.
- Berkhout, A.J., Wave field extrapolation techniques in seismic migration, a tutorial, Geophysics, 46, 1638-1656, 1981.
- Berryhill, J.R., Diffraction response for nonzero separation of source and receiver, Geophysics, 42, 1158-1176, 1977.
- Brown, R.J.S., Normal-moveout and velocity relations for flat and dipping beds and for long offsets, Geophysics, 34, 180-195, 1969.
- Claerbout, J. F., Coarse grid calculations of waves in homogeneous media with application to delineation of complicated seismic structure, Geophysics, 35, 407-418, 1970.
- Claerbout, J. F., Toward a unified theory of reflector mapping, Geophysics, 36, 467-481, 1971.
- Claerbout, J. F. and S. H. Doherty, Downward continuation of moveout corrected seismograms, Geophysics, 37, 741-768, 1972.
- Frazer, L.N., and J.A. Carter, Modeling zero offset reflection data for complex velocity models by summation over wavefronts, (abstract), EOS, Transactions, Am. Geophys. Union,
- French, W. S., Two-dimensional and three-dimensional migration of model experiment reflection profiles, Geophysics, 39, 265-277, 1974.
- French, W. S., Computer migration of oblique seismic reflection profiles, Geophysics, 40, 961-980, 1975.
- Gardner, G.H.F., W.S. French, and T. Matzuk, Elements of migration and velocity analysis, Geophysics, 39, 811-825, 1974.



- Gazdag, J., Wave equation migration with the phase-shift method, Geophysics, 43, 1343-1351, 1978.
- Hagedoorn, J.G., A process of seismic reflection interpretation, Geophys. Prosp., 2, 85-127, 1954.
- Hilterman, F.J., Three-dimensional seismic modeling, Geophysics, 35, 1020-1037, 1970.
- Hilterman, F.J., Amplitudes of seismic waves - a quick look, Geophysics, 40, 745-762, 1975.
- Hilterman, F.J., Interpretative lessons from three-dimensional modeling, Geophysics, 47, 784-808, 1982.
- Mitzner, K.M., Numerical solution for transient scattering from a hard surface of arbitrary shape - Retarded potential technique, J. Acoust. Soc. Am., 42, 391-397, 1967.
- Schneider, W., Integral formulation for migration in two and three dimensions, Geophysics, 43, 49-76, 1978.
- Stoffa, P.L., J.B. Diebold, and P. Buhl, Velocity analysis for wide aperture seismic data, Geophys. Prosp., 30, 25-57, 1982.
- Stolt, R. H., Migration by Fourier transform, Geophysics, 43, 23-48, 1978.
- Taner, M. T. and F. Koehler, Velocity spectra-digital computer derivation and application of velocity functions, Geophysics, 34, 859-881, 1969.
- Trorey, A.W., A simple theory for seismic diffractions, Geophysics, 35, 762-784, 1970.

## APPENDIX A

NOTES ON THE REAL-TIME APPLICATION  
OF KIRCHHOFF MIGRATION

While conducting a marine seismic reflection survey it is often important to have a good picture of the bottom morphology. SEAMARK II and SEABEAM are important tools for determining the morphology of an area but are not available to most scientific research vessels and lack the depth penetration obtainable using airgun or watergun sources. When traditional reflection methods are used, however, diffractions and displaced horizons may obscure the section and the data should be migrated before a clear picture of the morphology along the line can be obtained. Migration has always been a post-cruise processing procedure and thus, information which may be quite useful during the cruise is not obtained until the data have been returned. Usually, single channel data are not migrated even in post-cruise processing because the process can be time consuming and expensive. In this appendix I propose a method of obtaining preliminary near real-time migrations of single channel data. The method eliminates the necessity of post-cruise processing except in areas where more detailed results are desired.

The method I propose is based on a simplified version of the Kirchhoff migration routine described in the text of this dissertation. As described in the text, a velocity-depth function is required for the computation of the migration curves. Since it is difficult to obtain a good first guess of the velocity-depth function in real-time, a constant velocity is assumed. The water velocity is the obvious choice. The assumption of a constant velocity insures that the migration curves will always be the same for a particular

depth and thus need be computed only once, at the beginning of the line. The assumption also means that only the bottom reflection will be properly migrated; any subsurface reflector, although closer to its true position will be undermigrated (see APPENDIX B).

The proposed procedure for real-time migration is as follows. To begin the process, enough traces to fill the migration aperture (usually 25 to 49 traces) must be stored in the computer memory. When this has been accomplished, the data are summed along the pre-determined migration curves for the trace at the center of the aperture. The resulting migrated trace is output to a printer for immediate display. The next trace to be input replaces the oldest trace stored and the data are summed along the migration curves for the new center of the aperture and again output. This procedure may be followed as long as the speed of the ship and the source repetition rate remain constant. When either of these parameters change, the migration curves must be recalculated and the process begun again.

A certain amount of equipment is necessary to obtain real-time migrations. First, a sampling device must trigger on the outgoing pulse and sample the reflected returns during a pre-set time window. The computer must have enough memory to store 25 to 49 traces of data and must be able to sum over the migration curves and output the migrated trace before the next trace has been recorded (about 5 seconds). Finally, a plotter is needed for displaying the results. These are modest requirements and most scientific research vessels could be outfitted at reasonable expense.

## APPENDIX B

RAPID F-K MIGRATION OF ZERO OFFSET

MARINE REFLECTION DATA

A paper accepted for publication in the  
Journal of Geophysical Research, July, 1982

## RAPID F-K MIGRATION OF ZERO OFFSET MARINE REFLECTION DATA

Jerry A. Carter and L. Neil Frazer

Hawaii Institute of Geophysics, University of Hawaii,  
Honolulu, Hawaii 96822

Abstract. Recently developed frequency-wave number migration algorithms have made it possible to migrate digitally recorded zero-offset reflection data economically. The greatest contributions to the speed of these methods lie in the well-known symmetries of the Fourier transform and the assumption of a constant velocity section. Several problems have been addressed by using a newly proposed algorithm. The problem of incorrect phase shifts caused by the assumption of a two-dimensional medium is solved by utilizing a three-dimensional derivation of the theory. Another problem results from the assumption of a constant migration velocity. The parts of the record section with root mean square velocities less than the migration velocity will be overmigrated and the parts where the rms velocity is greater than the migration velocity will be undermigrated. Given a velocity-depth function, the rms velocity to a selected portion of a section is a good estimate of the velocity necessary to migrate that portion correctly. Errors in the rest of the migrated section can be reduced by applying the time-stretching formula of Stolt (1978) prior to migration. Beyond the spatial Nyquist frequency, aliasing noise can become a problem. The amount of aliasing is dependent upon the shot spacing, the frequency content of

the source, and the dip of the reflector. The shot spacings commonly in use today are sufficiently small to avoid spatial aliasing; however, shot spacings should be decreased when steeply dipping reflectors are expected and the source frequency is high. The use of automatic gain control before migration tends to reduce the signal-to-noise ratio of the migrated section and should be avoided if possible, especially for record sections with large areas of low reflection strength.

#### Introduction

The past few years have seen major advances in migration techniques. Several migration methods are commonly in use, each with its own advantages and disadvantages. Kirchhoff migration [Schneider, 1971; French, 1974; Schneider, 1978] has its origins in the Kirchhoff integral solution to the wave equation. Although this method works fairly well when velocity varies only with depth, its cost is proportional to the steepest dip that can be migrated. In finite difference migration [Claerbout, 1970; Claerbout and Doherty, 1972; Loewenthal et al., 1976], the wave equation is converted to a difference equation that is used to migrate the source-receiver pair down through the section. This method is perhaps the best one for dealing with two- and three-dimensional velocity depth functions but does not work well on steep dips and is slow. The phase shift method [Gazdag, 1978, 1981] works well with a depth dependent velocity function but requires a Fourier transform at each depth and is

therefore slow.

Perhaps the fastest running and easiest scheme to implement is the frequency-wave number (F-K) method [Stolt, 1978]. In this method, the assumption that velocity is constant allows the entire migration to be performed in one step in F-K space, so the number of Fourier transforms required is small. The major difficulty with F-K schemes is their inability to handle inhomogeneous velocities during migration, although pre-migration time stretches have been developed to mitigate this problem [Stolt, 1978]. The advantage of these schemes is that they are ideally suited for reducing large volumes of data quickly and accurately if the deviations from the migration velocity in the velocity-depth function are small.

In this paper we address some of the problems that can arise when F-K migration is used on single channel (or stacked multichannel) reflection data. These problems include incorrect phase shifts caused by use of a two-dimensional method to treat data gathered in a three-dimensional world, overmigration and undermigration because of errors in the velocity function used to migrate, spatial aliasing due to an insufficient density of shots or receivers, and the effects of automatic gain control when applied before migration.

#### Review of F-K Migration Theory

The kinematical theory of F-K migration originated with Stolt [1978], who obtained his algorithm from an imaging principle. Phinney and Frazer [1979] obtained a dynamically correct version of the Stolt



algorithm by means of a Born series solution of the wave equation. Neither the Stolt nor the Phinney and Frazer derivations will be repeated here, as our main interest is in the application of the theory and not its origin. Many of the details of F-K migration theory can be found in the tutorial article of Chun and Jacewitz [1981].

Using the notation of Phinney and Frazer [1979], we begin with an unprocessed, zero offset, time distance reflection record  $s(x,t)$ . The data are double Fourier transformed to obtain the section in wavenumber-frequency space  $S(\alpha,\omega)$ ,

$$S(\alpha,\omega) = \iint_{x t} e^{i(\alpha x + \omega t)} s(x,t) dx dt \quad (1)$$

We now perform a mapping from  $\alpha,\omega$  space into  $\alpha,\zeta$  space as illustrated in Figure 1. The mapping is governed by the equation

$$\zeta = (4\omega^2/c_0^2 - \alpha^2)^{1/2} \quad (2)$$

where  $c_0$  is the migration velocity so that lines of equal  $\omega$  in  $\alpha,\omega$  space appear as circles of radius  $2\omega/c_0$  in  $\alpha,\zeta$  space.

The mapping described in (2) implies a conversion from frequency to wavenumber or, in the time domain, a conversion from time to depth. However, because a constant velocity is used this is not a true conversion. So that the migrated sections are not confused with true depth sections, we plot the migrated sections in two-way travel time.

In practice, the migrated section  $M(\alpha, \zeta)$  must be determined at constant intervals of  $\zeta$ . Equation (2) can be rewritten

$$\omega = (\zeta^2 + \alpha^2)^{1/2} c_0 / 2 \quad (3)$$

With this  $\omega$ , the value of  $M$  at  $(\alpha, \zeta)$  is determined by interpolation of  $S(\alpha, \omega)$ . Note that  $\alpha$  and  $\omega$  are confined to the sector  $-2\omega/c_0 < \alpha < 2\omega/c_0$  by the range of  $\zeta$  (Figure 1). The complete mapping for the half plane  $\zeta > 0$  is given by

$$M^*(\alpha, \zeta) = \frac{\pi^{1/2} \gamma^{3/2} \omega^{-2} e^{-i\pi/4}}{A(\omega) D(\gamma, \gamma)} S(\alpha, \omega) \quad (4)$$

in which  $\gamma = \zeta/2$ . As will be shown later,  $M(\alpha, \zeta)$  need not be determined in the half plane  $\zeta < 0$ .  $A(\omega)$  is the Fourier transform of the source function and acts as a deconvolution operator. A directivity function  $D(\gamma, \gamma)$  has also been included in this derivation and can be used to deghost the data. For example, in the marine case where pressure is recorded and the source is an explosion,  $D(\gamma, \gamma)$  is set to  $4\sin(\gamma H)\sin(\gamma H')$  where  $H$  and  $H'$  are the source and receiver depths, respectively, so that the free surface bounce at the source and receiver will be deconvolved. Both the source and the directivity functions have been set to unity for the examples shown later in this paper. Equation (4) was obtained by Phinney and Frazer [1979] through a steepest descent evaluation of the integral for three-dimensional imaging. The only assumption necessary was that scatterers be many

wavelengths below the surface on which the data are gathered; then near-field terms can be dropped from the radiation patterns of the source and scatterers.

The migrated section is obtained by double inverse Fourier transformation.

$$m(x, z) = (z)^{1/2} (2\pi)^{-2} \iint_{\alpha \zeta} M(\alpha, \zeta) e^{i(\alpha x + \zeta z)} d\alpha d\zeta \quad (5)$$

Ignoring  $A(\omega)$  and  $D(\gamma, \gamma)$ , (4) differs from the derivation of Stolt [1978] by an extra factor of  $2(z\pi\gamma)^{1/2} e^{i\pi/4} (\omega c_0)^{-1}$ . This factor originates from the assumption of three-dimensional wave propagation for two-dimensional migration as opposed to Stolt's derivation in which two-dimensional propagation is assumed. The important term in (4) is the exponential which, because it is left out of Stolt's derivation, leads to a phase shift of  $-\pi/4$ . A synthetic record section for a point scatterer is shown in Figure 2a. The source used was a zero phase wavelet; its derivative appears in the synthetics because a point scatterer acts as a differentiator. In Figure 2b the hyperbola in Figure 2a has been migrated using Stolt's algorithm, and in Figure 2c we show the result of migrating with Phinney and Frazer's scheme. Although both methods have collapsed the hyperbola, the phase shifts associated with Stolt's derivation have distorted the output wavelet. The small amount of distortion present in Figure 2c is thought to be due to the finite length of the wavelet. Except for Figure 2b, all of the migrations shown in this paper were done with

equation (4).

### The Two-Dimensional FFT

Much of the CPU time in F-K migration involves the two two-dimensional fast Fourier transforms (FFTs), especially when the computer being used is not equipped with an array processor. In this section we discuss some methods, derived from the theory of discrete Fourier transforms, for reducing the CPU time. Additional timesaving methods are largely dependent on the machine being used and the user's ability to manipulate large data sets.

Consider a data set  $s(x,t)$  of  $n$  rows and  $m$  columns (Figure 3a). To double Fourier transform the data set twice (once forward and once inverse)  $2(n+m)$  discrete finite functions must be transformed. However, by taking advantage of the symmetry properties of the Fourier transform, [e.g., Brigham, 1974], this number can be reduced by nearly half.

We begin by transforming the columns of the data set. The choice of columns is arbitrary; it is just as valid to start with the rows. A property of the Fourier transform is that the transform of a real function is hermitian (its real part is an even function and its imaginary part is an odd function) and the transform of a purely imaginary function is antihermitian (the real part is odd and the imaginary part is even). As any function is easily split into its even and odd parts, it is also easy to separate a complex function into its hermitian and antihermitian parts. Thus if we combine two

real functions (columns)  $s(x_{2k}, t)$  and  $s(x_{2k-1}, t)$  into a single complex function  $r(x'_k, t) = s(x_{2k}, t) + is(x_{2k-1}, t)$  as in Figure 3b and then Fourier transform  $r$  with respect to  $t$  we obtain  $\hat{r}(x'_k, \omega)$  (Figure 3c). The hermitian part of  $\hat{r}$  is the Fourier transform of  $s(x_{2k}, t)$  and the antihermitian part of  $\hat{r}$  is the Fourier transform of  $s(x_{2k-1}, t)$  (Figure 3d). Because the transforms can be computed two at a time, the number of transform computations has been reduced by a factor of 2.

Now note that the negative frequencies of the transformed array are the complex conjugates of the positive frequencies, i.e.,  $\hat{s}(x, -\omega) = \hat{s}^*(x, \omega)$ . This fact is symbolized in Figures 3c-h by representing the negative frequency half of the array by the complex conjugate of the positive frequency half. Except at the zero and Nyquist frequencies, each row has a complex conjugate row. The Fourier transform of the complex conjugate of a function  $\hat{s}(x, \omega)$  is  $S^*(-\alpha, \omega)$ , so by transforming the positive, zero, and Nyquist frequency rows all of the information contained in the fully transformed array is obtained (Figure 3e). It is not necessary to store the negative frequency part of the array in steps d-g as it may be generated from the positive frequencies in step h. In Figure 3 the shaded boxes represent the frequencies that need not be stored.

The array has now been doubly Fourier transformed in only  $(m/2) + (n/2) + 1$  transforms, and we now do the migration mapping as described by (4) and Figures 1 and 3f. This step involves an interpolation that can be carried out by a number of methods (e.g.,

linear, cubic spline, sinc). Better accuracy is obtained by using the more complicated interpolation methods, but because the frequencies dealt with in this paper are well below the sample Nyquist frequency the linear scheme is sufficient. With the mapping completed, we are ready to doubly inverse transform the array  $M(\alpha, \zeta)$  from  $\alpha, \zeta$  space to  $x, z$  space. The same methods that were used above can be applied in reverse to obtain the migrated section.

The first inverse transformation is simple; there are only  $(n/2)+1$  rows and inverse transformations are performed on all of them to obtain  $\hat{m}(x, \zeta)$  (Figure 3g). For the final transformation two complex column functions  $\hat{m}(x_{2k}, \zeta)$  and  $\hat{m}(x_{2k-1}, \zeta)$  are combined into a single function  $\hat{p}(x'_k, \zeta) = \hat{m}(x_{2k}, \zeta) + i\hat{m}(x_{2k-1}, \zeta)$  as in Figure 3h. When  $\hat{p}(x'_k, \zeta)$  is inverse transformed, a complex function  $p(x'_k, z)$  will be obtained in which the real part is the inverse transform of  $\hat{m}(x_{2k}, \zeta)$  and the imaginary part is the inverse transform of  $\hat{m}(x_{2k-1}, \zeta)$  (Figure 3i). The final step is to generate the real array  $m(x, z)$  from  $p(x', z)$  (Figure 3j). As in the forward transformations, we have performed just  $(m/2)+(n/2)+1$  transforms in the inverse case. The total number of transformations has been reduced from  $2(n+m)$  to  $n+m+2$ .

A few practical limitations should be considered when using the methods described above. Most important is the tendency of Fourier transformed data to wrap around on itself. For example, a reflector that ends abruptly at the edge of a record section wraps around onto the opposite edge of the section after migration. Wrap-around can be avoided by adding extra data to the bottom and sides of the array. If

the extra data are not available, the array should be smoothly tapered to zero and zeros added instead. Theoretically, the amount of extra data or zeros added should result in a doubling of each dimension of the array. However, in practice, often much less than this amount is sufficient. For marine data the two-way travel-time through the water column must be included in each trace and usually contains enough zeros to eliminate the need for extra data or zeros at the bottom of the array.

The F-K migration method described above was applied to a physical model of a reef, provided by Southern Methodist University (SMU) (Figure 4). Model data rather than field data were used for better control of the structure to be migrated. The data were collected at SMU by employees of the Mobil Exploration Services Center by using a modeling apparatus at SMU. Figures 4a-4c show the model structure, the data set collected, and the migrated section. Interpretation of this section has been made much easier by migration. The lateral extent of the reef has been well defined and more important, the phase of the arrivals has been preserved. Without the preservation of phase, the correct interpretation of the reef edges would be difficult, as the reflection coefficient changes sign several times as the waves travel down the edges of the reef. The section required a two-dimensional array of 2048 time points by 256 shots and took roughly 4 minutes of CPU time to process on a HARRIS 800 computer without the aid of an array processor. The HARRIS 800 has a Whetstone number of 1470.

### Overmigration and Undermigration

Probably the most important input to F-K migration is the migration velocity. If the velocity used is too low, then the reflection hyperbolas will not completely collapse; the result is an undermigrated section. Conversely, if the velocity used is too large, then the limbs of the hyperbolas will migrate through the point reflector into 'smiles' and the record section is said to be overmigrated [e.g., Schultz and Sherwood, 1980]. Overmigration and undermigration can also be caused by use of incorrect sample rates and/or shot spacings.

We illustrate the problem of incorrect migration velocities in Figure 5. The point reflector synthetic section of Figure 5a was generated by using geometric principles. Zero phase wavelets were used with amplitudes proportional to the inverse of distance from the reflector. The shot spacing is 50 m, the sample rate is 200 Hz, and the velocity of the medium is 2.0 km/s. Two point reflectors, at 2- and 4-km depth with source center frequencies of 12.5 Hz, are shown.

In Figure 5b the section shown in Figure 5a has been migrated using a velocity of 1.8 km/s (a 10% undermigration). Only a small portion of the section is shown so that the features are more easily observed. In both cases, the hyperbolas have not been completely collapsed into their respective point reflectors and each has been subjected to an apparent  $-\pi/4$  phase shift, slightly displacing them from their actual positions. In addition, there are noticeable differences between the migrated shallow and deep reflectors. The shallow reflector is less



dispersed than the deep reflector. We attribute this to the fact that in the unprocessed section proportionately more energy is concentrated at the apex of the shallow point reflector than at the apex of the deep point reflector.

A migration velocity of 2.2 km/s was used in Figure 5c to demonstrate the effects of a 10% overmigration. The energy in the diffraction patterns has been migrated through the point source into 'smiles' that have an apparent phase shift of  $+\pi/4$ ; the opposite direction as in the undermigration case. As in the undermigration case, near-surface reflectors are less susceptible to migration velocity errors than deep reflectors.

Figure 5d shows the results of migrating the section at the correct velocity of 2.0 km/s. All of the energy has been collapsed into the image points and no phase shifting has occurred.

#### Velocity-Depth Functions

Much attention has been given to the problem of implementing velocity depth functions in Fourier transform migration routines [e.g., Gazdag, 1978, 1981; Chun and Jacewitz, 1979]. Unfortunately, many of these methods are time consuming and are not well suited for routine processing of large amounts of data. There are two methods that are ideally suited for the type of applications addressed in this paper. Both utilize the rms velocity.

In all F-K migration routines, the diffraction patterns associated with each subsurface point are assumed to be hyperbolas. At a given

depth in a layered medium an excellent approximation to the diffraction pattern is defined by the rms velocity [Taner and Koehler, 1969]. The rms velocity is given by

$$v_{\text{rms}}^2 = \frac{1}{T} \int_0^T dt c^2(t) \quad (6)$$

where  $T$  is the one-way travel time to the interface of interest and  $c(t)$  is the velocity-depth function. If we define a portion of the data in need of migration, then the rms velocity to that portion may be used as the migration velocity. Of course, all other portions of the section will be either undermigrated or overmigrated depending on their rms velocity. This method is illustrated in Figure 6. The synthetic section in Figure 6a consists of two layers overlaying a 4.0 km/s half-space with a point scatterer in each layer. In Figure 6b the section has been migrated by using the rms velocity to the lower point scatterer (1.665 km/s). The upper diffraction pattern has been overmigrated as expected and the lower pattern has been nearly completely collapsed.

A slightly more difficult procedure follows the time shifting methods of Stolt [1978]. In Stolt's method, a time transform is defined that maps all diffraction patterns into approximations of the hyperbolas that would be generated by scatterers in a medium of constant velocity  $v$ . Let  $s(x,t)$  be the original record section and  $s'(x,t)$  the transformed record section. Then the transform is

$s'(x, t_n) = s(x, t)$ , where

$$t_n = \left( \frac{2}{v} \int_0^t v_{\text{rms}}^2(t) t dt \right)^{1/2} \quad (7)$$

In this equation,  $v_{\text{rms}}$  is regarded as a function of vertical two-way travel time and  $v$  is the constant velocity to be used later in the F-K migration.  $v$  is usually chosen to minimize the difference between  $t_n$  and  $t$ . An application of Stolt's method is shown in Figure 6c. Although the lower diffraction pattern has not been migrated perfectly, the overall result is much better than the migration using the rms velocity.

For single channel marine reflection records we have found that migration at the water column velocity is most useful for general data processing. Bathymetric features perpendicular to the line are correctly migrated and deeper reflections, although undermigrated, are enhanced. In addition, no a priori knowledge of the velocity-depth function is necessary. If desired, the section can be remigrated at a velocity that will improve the appearance of the deep structure. Linear bathymetric features that cross the line obliquely can be enhanced by the use of a higher migration velocity which depends on the angle of the feature to the line [French, 1975].

#### Spatial Aliasing

Another important consideration when migrating reflection data is

spatial aliasing. Johnson [1980] has described the noise attributable to aliasing in migration and Larner et al. [1981] attempt to solve the aliasing problem by interpolating traces between the aliased ones under certain conditions. In this section we illustrate the effects of spatial aliasing as a function of the shot spacing for a point scatterer.

Spatial aliasing is directly related to the wavelength of the signal being migrated, the spacing of the shots, and the dip of the reflector. For spatial aliasing to occur  $\Delta x > \cot(\theta) c/(2f)$ ; where  $c/(2f)$  is one-half the wavelength of the reflection,  $\theta$  is the dip of the reflection, and  $\Delta x$  is the shot spacing. Thus, a trade-off exists between the frequency of the source and the shot spacing. For instance, a 10-Hz source signal fired at 100-m intervals would produce aliasing at the same dip as a 20-Hz source fired every 50 m, or a 5-Hz source at 200-m intervals. In the following examples, the source center frequency is kept constant at 25 Hz and the shot spacing is varied. A point 250 m below the surface is used as the reflector. In Figure 7, the distance from the apex of the hyperbola where spatial aliasing begins is shown by arrows for various values of  $\Delta x$ .

Assuming a realistic ship speed of 5 m/s (10 knots) and a 20 s/shot shot schedule, the shot spacing is 100 m. Figure 7a shows the synthetic data that would be observed under these conditions and the migrated section. The traces at 100 m are beyond the aliasing limit. Migration has not collapsed the hyperbolas in this case. Decreasing the shot spacing to 50 m by decreasing the shot schedule to 10 s/shot

eliminates aliasing near the apex, but it becomes a problem between 50 and 100 m on either side of the reflector. The hyperbola has been collapsed to a point, but energy appears on either side of the point reflector beyond 100 m (Figure 7b). Decreasing the shot spacing still further to 25 m (a 5-second schedule) pushes the aliased portions out to 187 m from the apex. In this case the aliasing noise is 24 dB below the level of the signal.

This example has been designed to demonstrate perhaps the worst conditions that will be encountered by using traditional marine reflection methods. If the frequency of the source had been lower than that used in the example, the shot spacings could have been correspondingly larger to produce the same results. In addition, had the reflector been deeper in the section, there would have been much less spatial aliasing.

#### Automatic Gain Control

Automatic gain control (AGC) is often used to reduce the dynamic range of reflection record sections before plotting. In the AGC process each seismic trace  $s(t)$  is replaced by  $s(t)/f(s,t)$  where  $f(s,t)$  is the square root of the energy of  $s(t)$  within a window centered at  $t$ . The undesirable nonlinear effects of AGC are minimized by using a window that tapers smoothly to zero, along with its derivative, at both ends.

When AGC is used the amplitude information necessary to determine acoustic impedance contrasts is lost, but the outline of the

subsurface structure may be enhanced. As an example, we use the model reef section of Figure 4; an AGC with a 0.4-s cosine window was applied to the data in Figure 4b to obtain Figure 8a. The migrated AGC'd section is shown in Figure 8b. As before, the reef structure has been made more readily apparent through the migration process. The structure at the right edge of the reef is better defined in the section that was AGC'd before migration (Figure 8b) than in the section that was not AGC'd before migration (Figure 4c). This structure has been enhanced because, before migration, the energy from its reflectors was distributed over a large area containing no other arrivals. On the other hand, the structure at the left edge of the reef is more poorly resolved in the section which was AGC'd before migration, particularly the lower reflectors on that edge. Away from the reef where the reflectors are flat and the energy was not laterally dispersed, there is no improvement and the signal-to-noise ratio has decreased. Also, the reflector-free regions to the right and left of the reef are noisier in the section that was AGC'd before migration. It thus appears that the effects of AGC before migration are unpredictable and that, if possible, it is better to AGC after migration rather than before.

The example used here is perhaps an extreme one because of its simple structure. Most seismic data have a more uniform distribution of reflected energy throughout the seismic section, and for such data the effects of AGC before migration will be less severe.

### Conclusions

Among academic institutions to which zero-offset reflection data are available there is a general need for a fast migration method that can be implemented as part of the standard reduction process. F-K migration routines offer such a capability and have the added advantage that deconvolution can be performed at the same time. Their disadvantage is an inability to handle complex velocity-depth functions accurately. Overmigration and undermigration cannot be avoided when the velocity-depth function is complex. However, by migrating at the rms velocity to the feature of interest or using the pre-migration time shifting methods of Stolt [1978], a great improvement in the data can be obtained.

Spatial aliasing is a concern of everyone involved in the processing of seismic reflection data. Although F-K migration methods are probably the most accurate up to the spatial Nyquist frequency, beyond that frequency aliasing noise can become a problem. In areas where dips are steep, spatial aliasing noise may be avoided by using a lower frequency source, decreasing the shot spacing, or filtering before migration.

The use of automatic gain control before migration results in a decreased signal to noise ratio and should be avoided if possible.

Acknowledgments. We thank Mat Yedlin for help with the development of the fast Fourier transform routines used in the F-K migration program and for informative discussions on the subject of migration.

We also thank R.H. Stolt for help in understanding his time transformation (equation (7)) and M.S. Redeker of the Mobil Exploration Services Center for providing the physical model data. Critical comments by Tom Brocher, Al Rudman, and two anonymous reviewers were helpful in revising the manuscript. This research was funded by the Ocean Acoustics program of the Office of Naval Research. Hawaii Institute of Geophysics contribution no. 1298.

#### References

- Brigham, O. E., The Fast Fourier Transform, Prentice-Hall, Englewood Cliffs, N. J., 1974.
- Chun, J. H., and C. A. Jacewitz, A fast multivelocity function frequency domain migration (abstract), Geophysics, 44, 328, 1979.
- Chun, J. H., and C. A. Jacewitz, Fundamentals of frequency domain migration, Geophysics, 46, 717-733, 1981.
- Claerbout, J. F., Coarse grid calculations of waves in homogeneous media with application to delineation of complicated seismic structure, Geophysics, 35, 407-418, 1970.
- Claerbout, J. F., and S. H. Doherty, Downward continuation of moveout corrected seismograms, Geophysics, 37, 741-768, 1972.
- French, W. S., Two-dimensional and three dimensional migration of model experiment reflection profiles, Geophysics, 39, 265-277, 1974.
- French, W. S., Computer migration of oblique seismic reflection profiles, Geophysics, 40, 961-980, 1975.
- Gazdag, J., Wave equation migration with the phase-shift method, Geophysics, 43, 1343-1351, 1978.
- Gazdag, J., Migration by phase shift plus interpolation in inhomogeneous media (abstract), Geophysics, 46, 408, 1981.
- Johnson, D. A., Practical aspects of frequency-wavenumber domain migration (abstract), Geophysics, 45, 515-516, 1980.



- Larner, K., B. Gibson, and D. Rothman, Trace interpolation and the design of seismic surveys (abstract), *Geophysics*, 46, 407, 1981.
- Loewenthal, D., L. Lu, R. Roberson, and J. Sherwood, The wave equation applied to migration, *Geophys. Prospect.*, 24, 380-399, 1976.
- Phinney, R. A., and L. N. Frazer, On the theory of imaging by Fourier transform, Paper presented at the 48th Annual Meeting of the Society of Exploration Geophysicists, San Francisco, October 1979.
- Schneider, W., Developments in seismic data processing and analysis (1968-1970), *Geophysics*, 36, 1043-1073, 1971.
- Schneider, W., Integral formulation for migration in two and three dimensions, *Geophysics*, 43, 49-76, 1978.
- Schultz, P. S., and J. W. C. Sherwood, Depth migration before stack, *Geophysics*, 45, 376-393, 1980.
- Stolt, R. H., Migration by Fourier transform, *Geophysics*, 43, 23-48, 1978.
- Taner, M. T., and F. Koehler, Velocity spectra-digital computer derivation and applications of velocity functions, *Geophysics*, 34, 859-881, 1969.

(Received February 1, 1982;  
revised July 12, 1982;  
accepted July 12, 1982.)

Copyright 1982 by the American Geophysical Union.

Paper number 2B1206.  
0148-0227/82/002B-1206 05.00

Fig. 1. The mapping from  $\alpha, \omega$  space to  $\alpha, \xi$  space (after Phinney and Frazer [1979]). Data along the horizontal lines in the  $\alpha, \omega$  plane are mapped into corresponding circles in the  $\alpha, \xi$  plane.

Fig. 2. Incorrect phase shifts caused by incorrect dynamical factors. The hyperbola in (a) is migrated by using Stolt's [1978] two-dimensional algorithm to obtain (b) and using Phinney and Frazer's [1979] scheme to obtain (c).

Fig. 3. A schematic diagram of F-K migration. Details are given in the text.

Fig. 4. A physical model is used to demonstrate the accuracy of the F-K migration method. (a) The reef model. (b) Data section collected from the model. (c) An F-K migration of the model data. Phase is preserved in this F-K method, making the interpretation easier near the edges of the reef where the sign of the reflection coefficient changes frequently.

Fig. 5. The effects of incorrect migration velocities. (a) A synthetic record section of point reflectors at 2- and 4-km depth in a 2.0-km/s medium. The center frequency of the source is 12.5 Hz. (b) Migration of (5a) at 1.8 km/s (10% undermigration). (c) Migration of (5a) at 2.2 km/s (10% overmigration). (d) Migration of (5a) at 2.0 km/s.

Fig. 6. Three-layer velocity-depth function with point reflectors in layers 1 and 2. (a) Synthetic section of the model. (b) Migration of (6a) at the rms velocity to the lower point reflector, 1.665 km/s. (c) Migration of (6a) after correcting to a constant velocity using Stolt's [1978] time shift method (equation (5)).

Fig. 7. Unmigrated (left column) and migrated (right column) sections of a point reflector at 250-m depth in a half-space of 1.5 km/s material. The 25-Hz source has spacings of (a) 100, (b) 50, and (c) 25 m to show the effects of spatial aliasing. The arrow on each section in the left-hand column indicates the offset beyond which the signal will be aliased.

Fig. 8. The effects of automatic gain control (AGC) prior to migration. (a) The unmigrated record section of Figure 4b after energy equalization (AGC) within a 0.4-s cosine window. (b) A migration of the AGC'd section in (a). This migrated section should be compared with the one in Figure 4c.

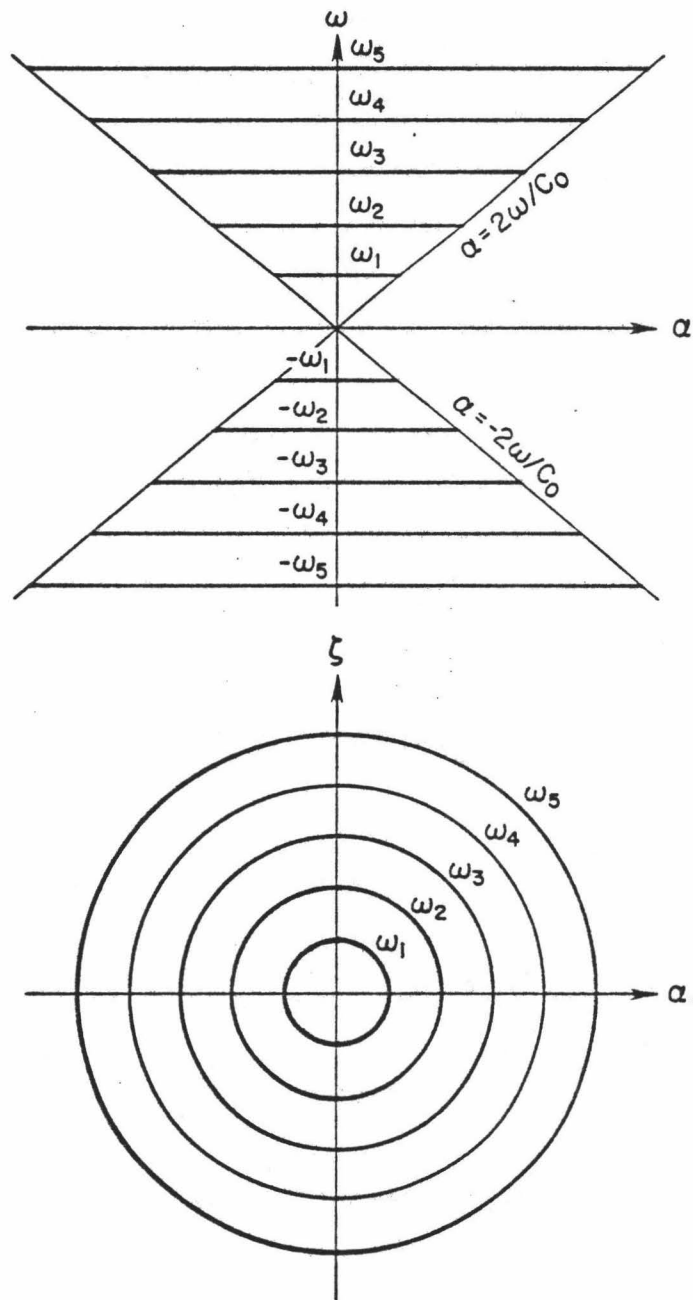


Figure 1

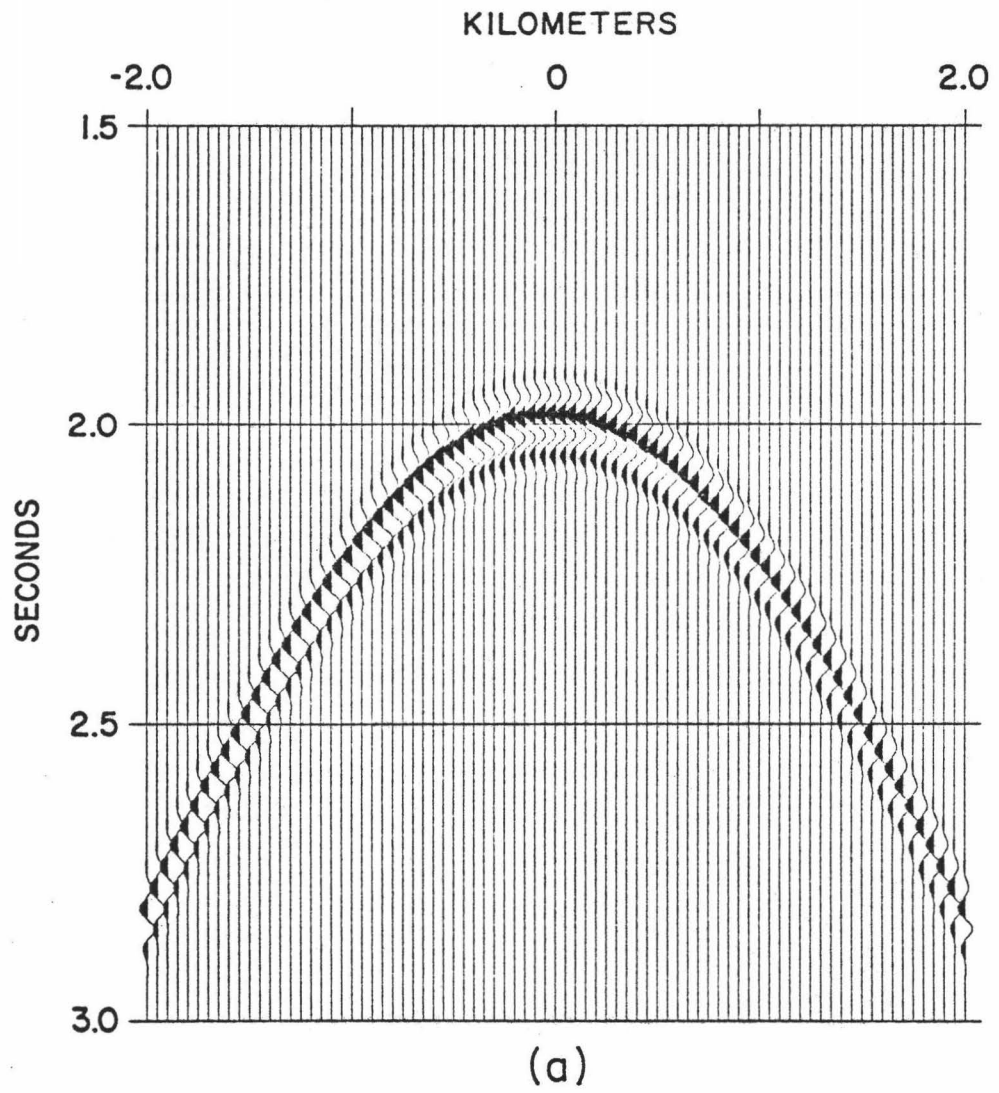


Figure 2a

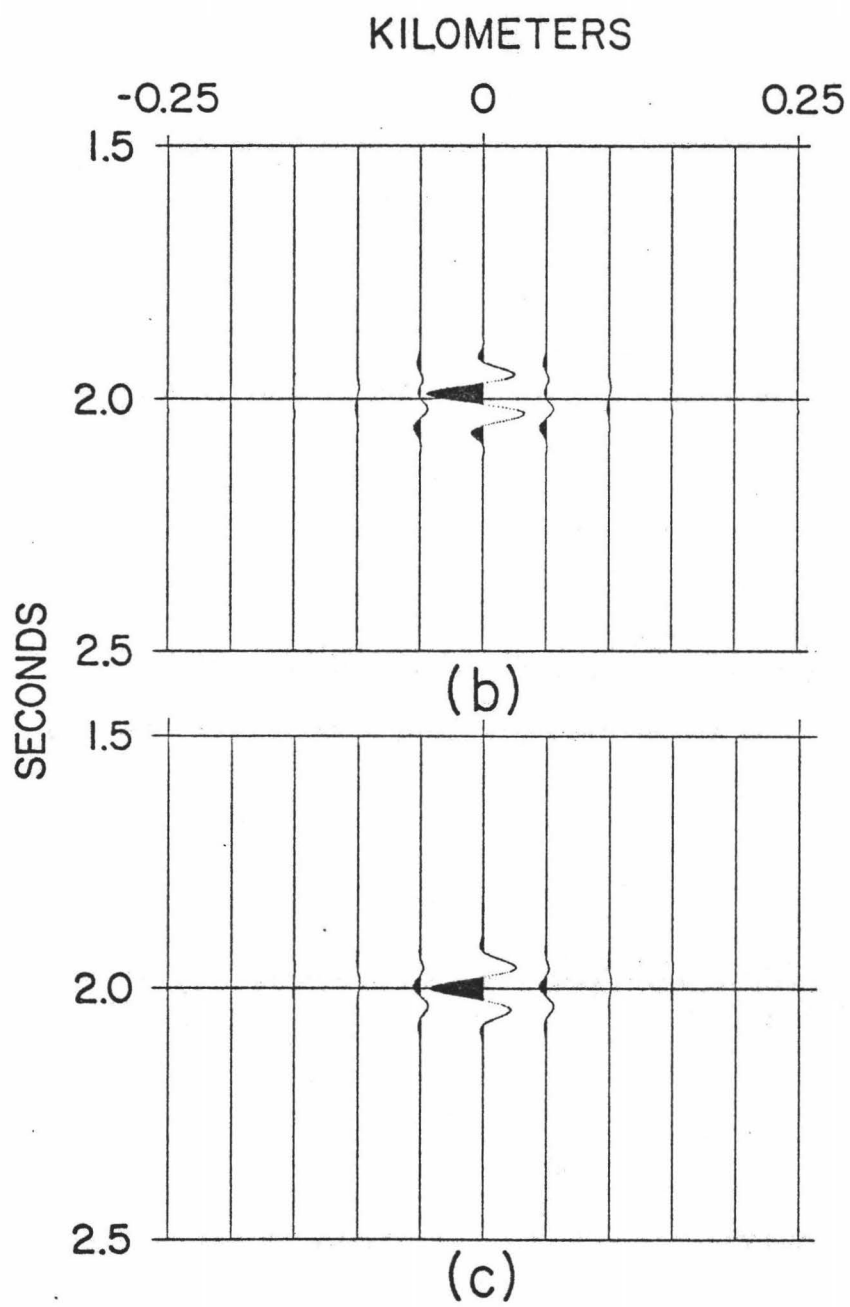


Figure 2b,c

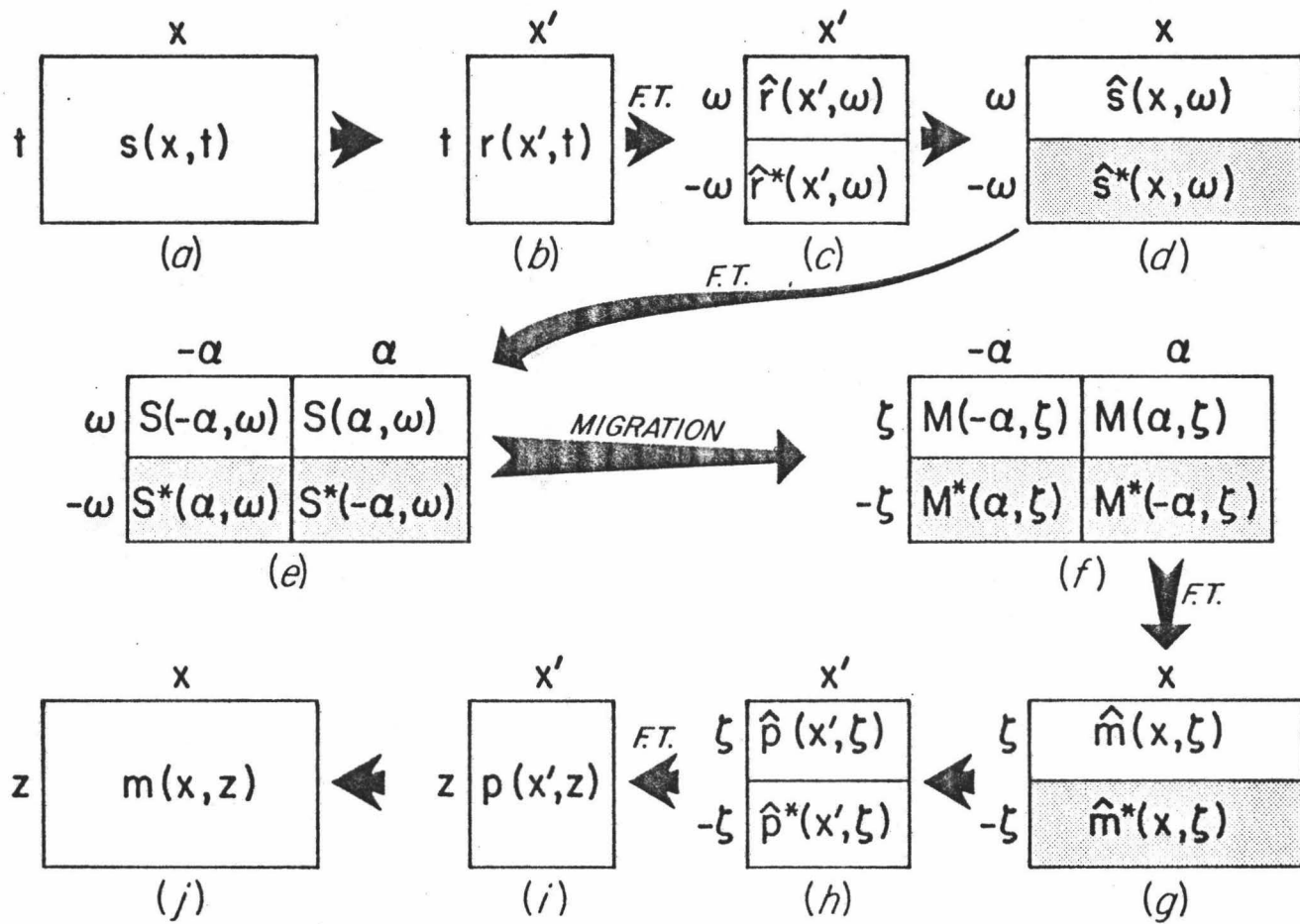
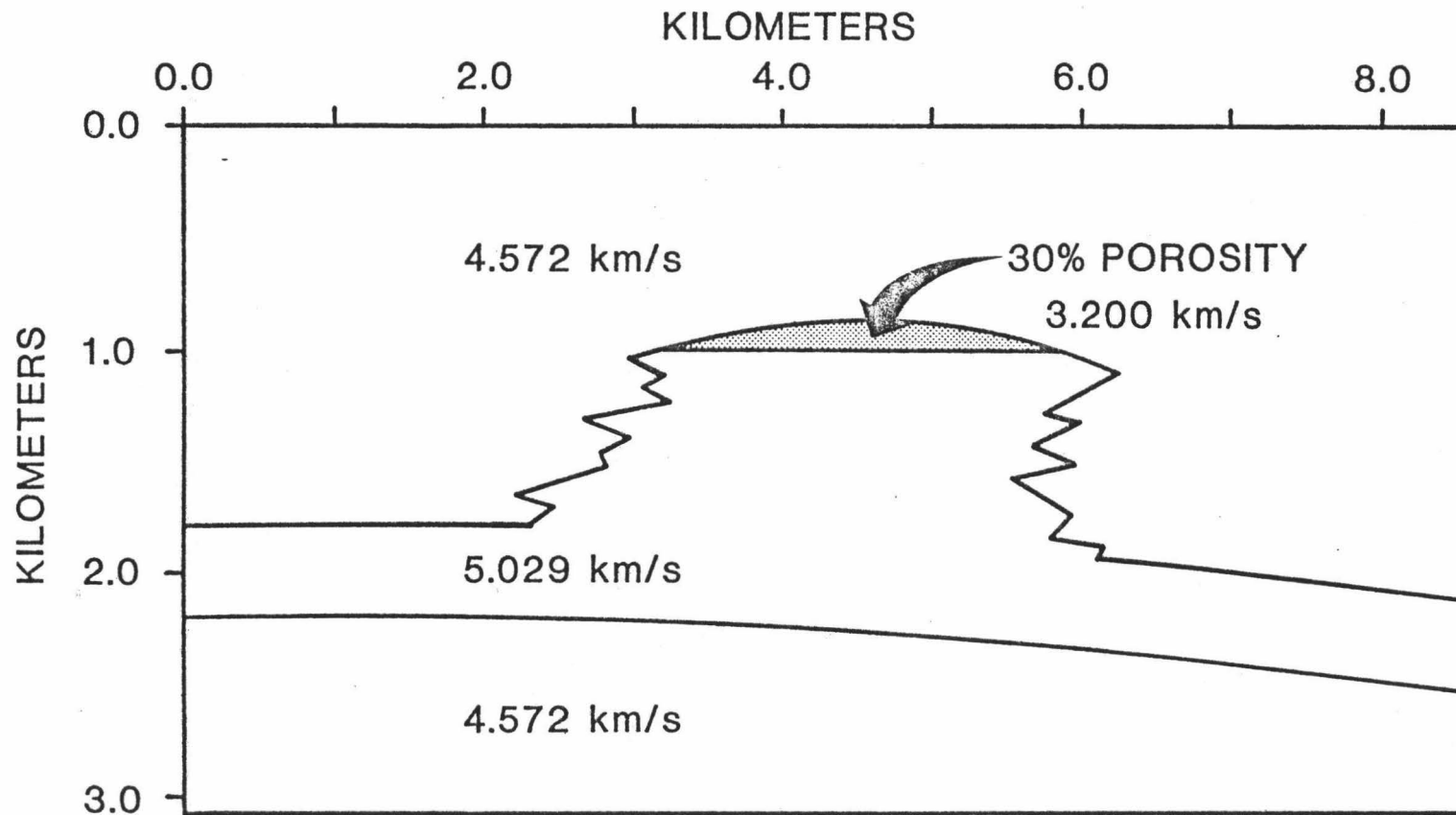
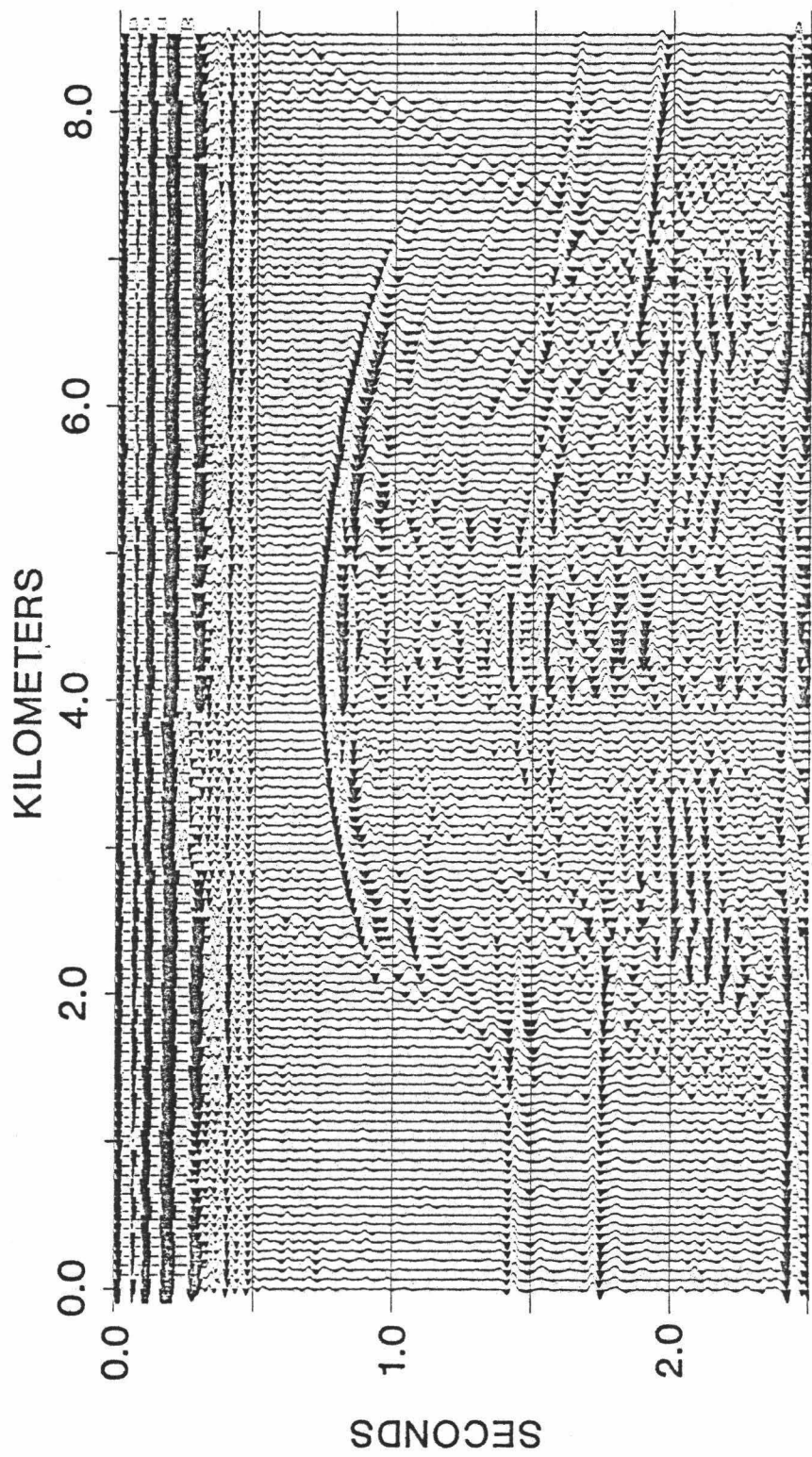


Figure 3



(a)

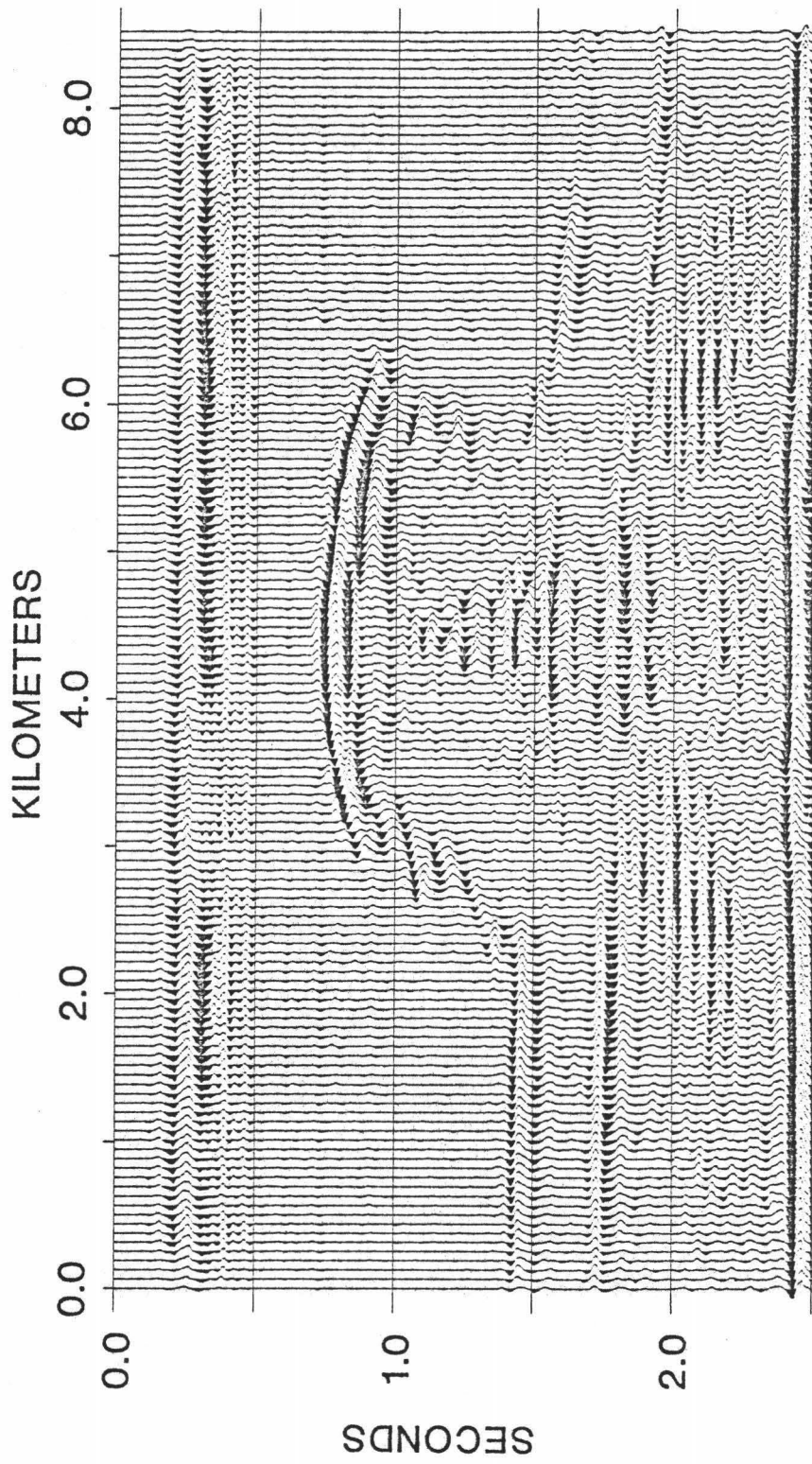
Figure 4a



(b)

Figure 4b





(c)

Figure 4c

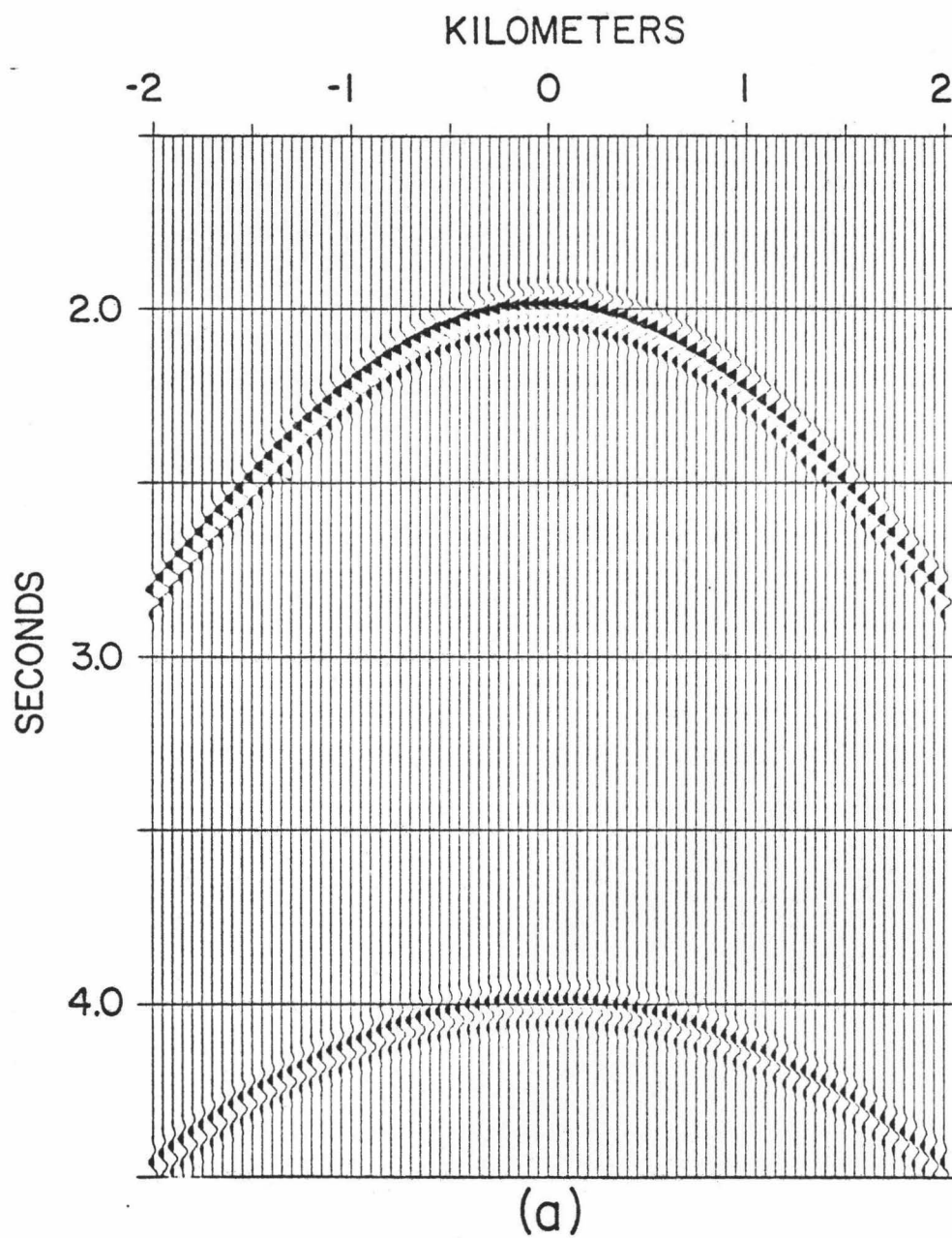


Figure 5a

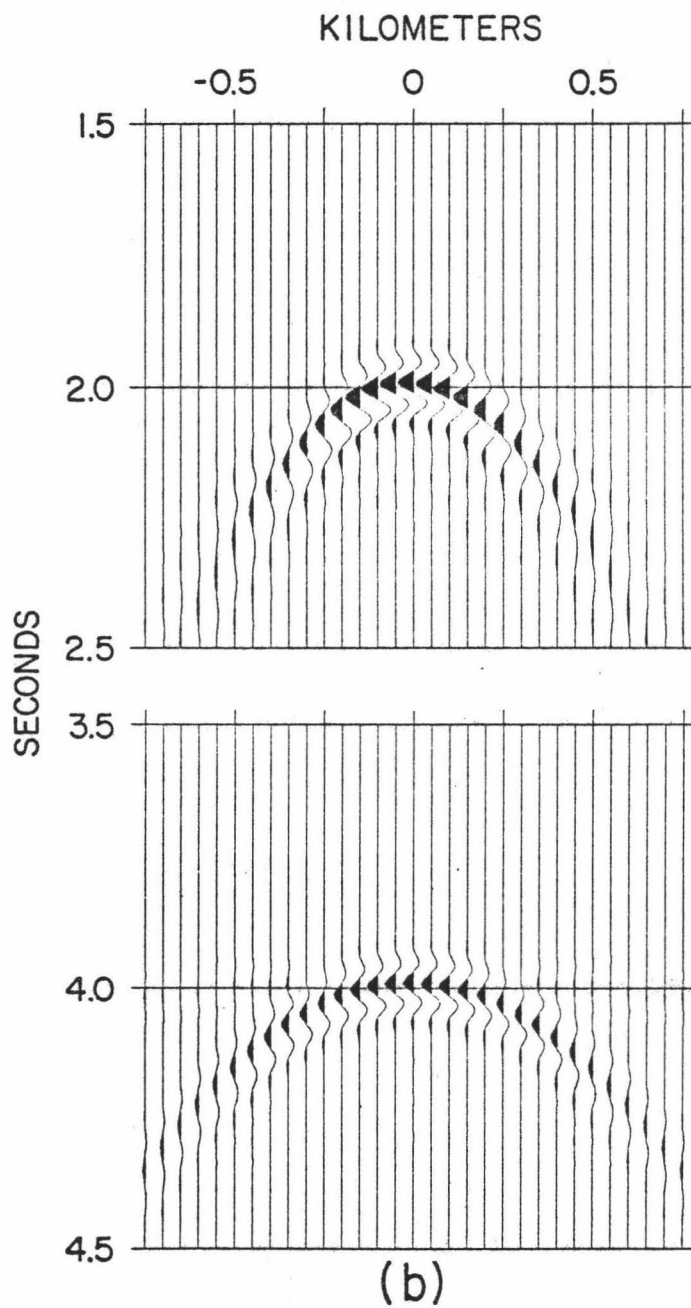


Figure 5b

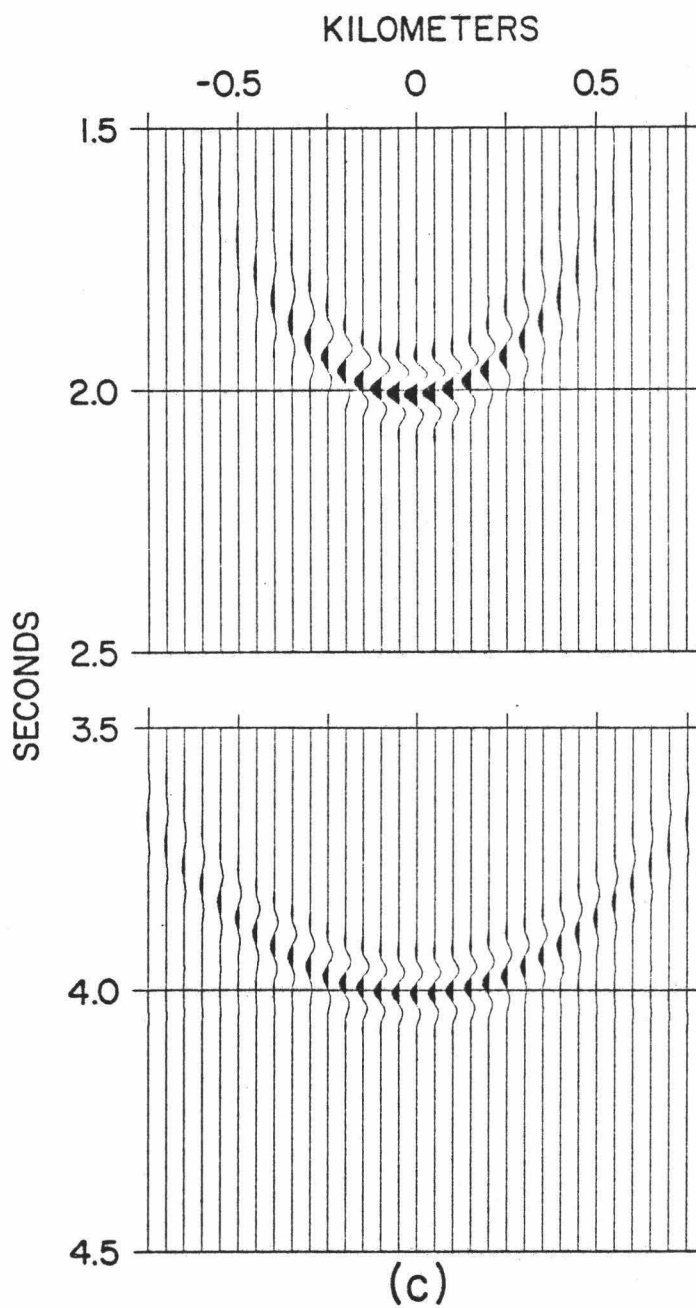


Figure 5c

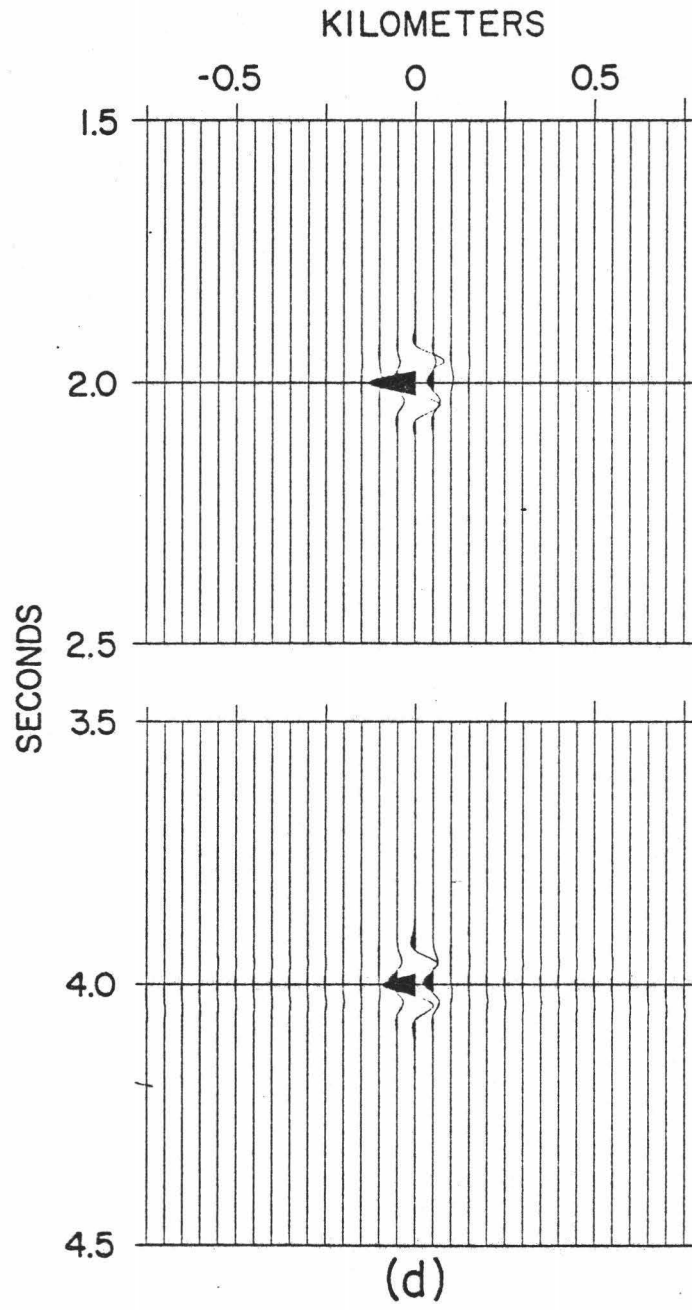


Figure 5d

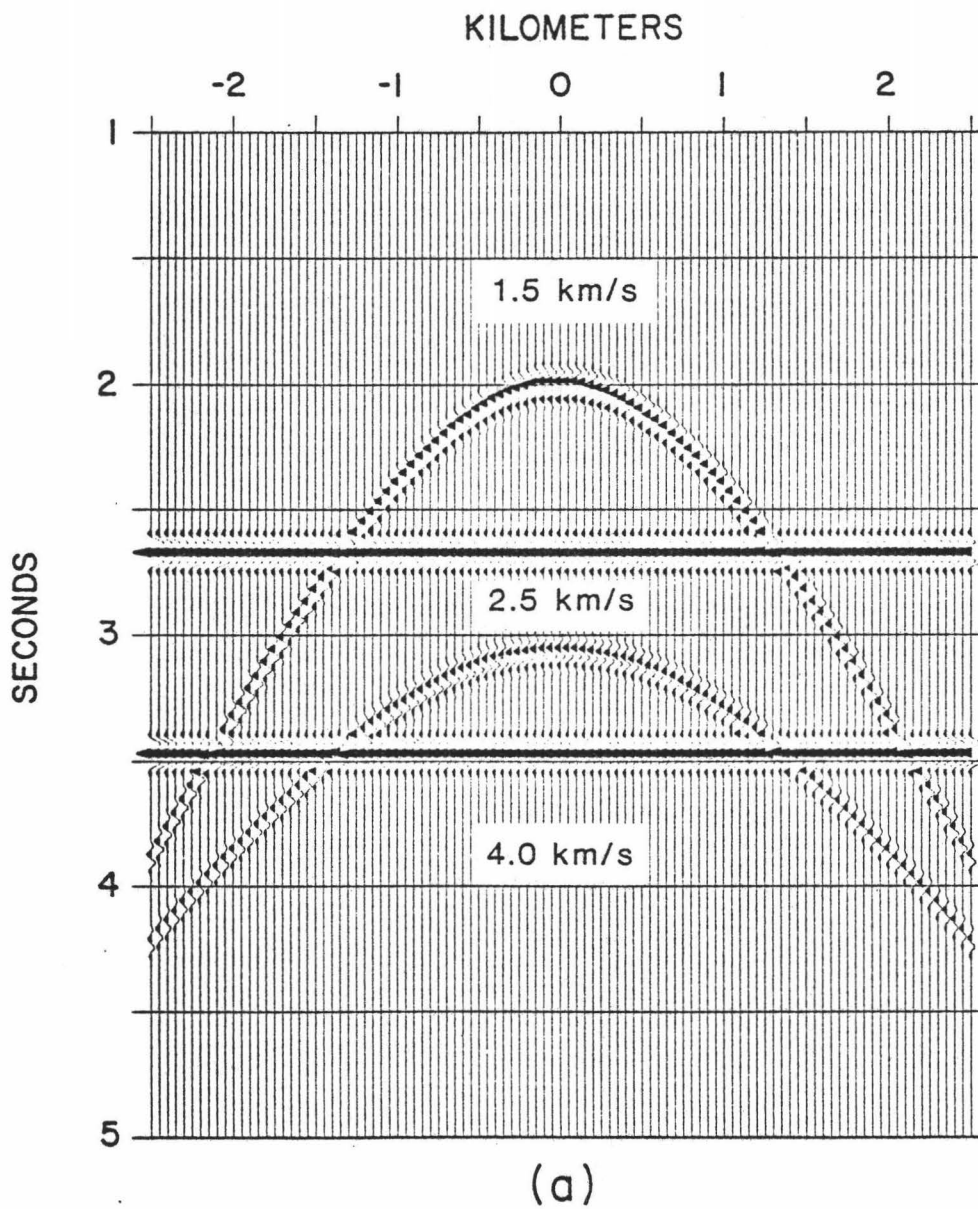


Figure 6a

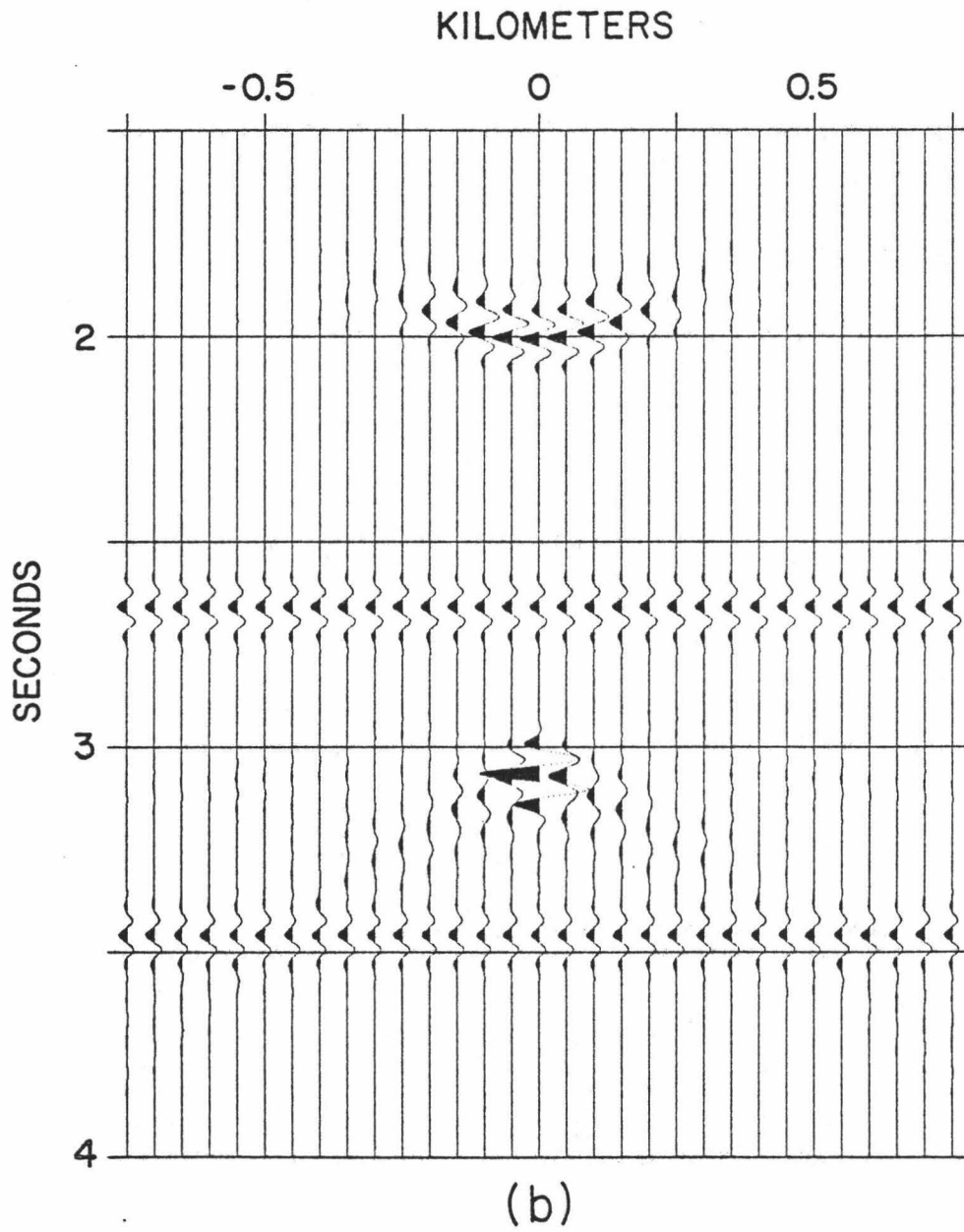


Figure 6b

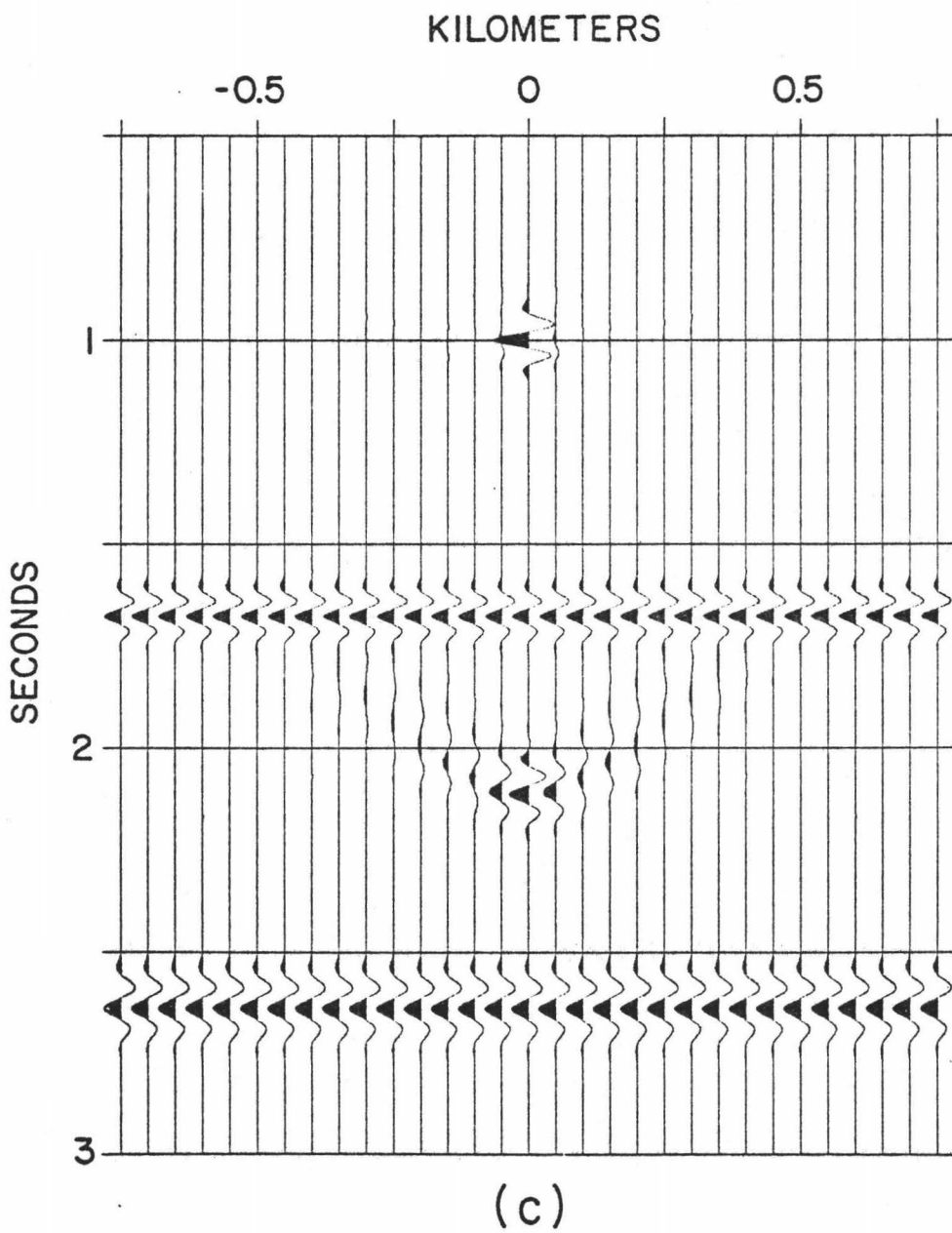


Figure 6c



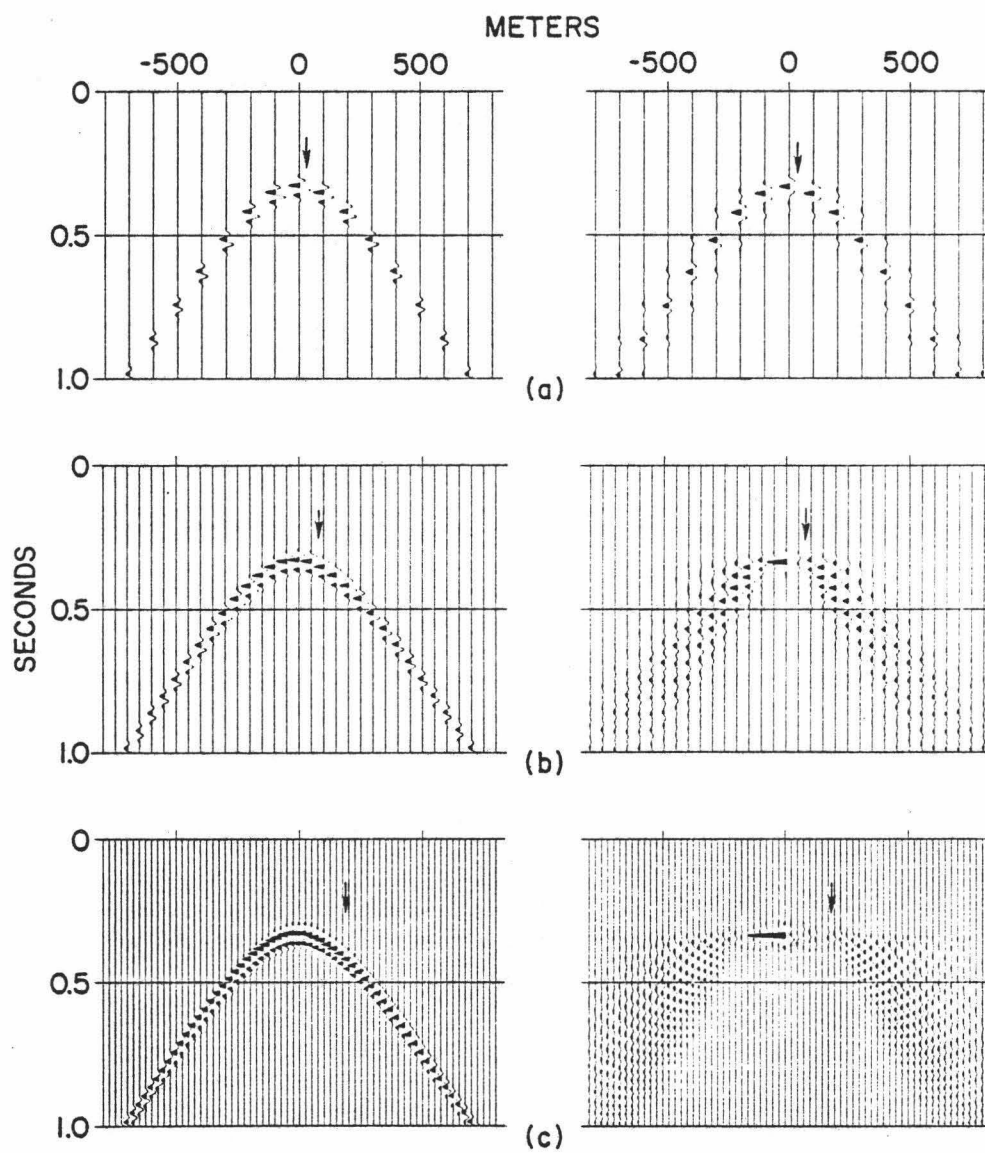
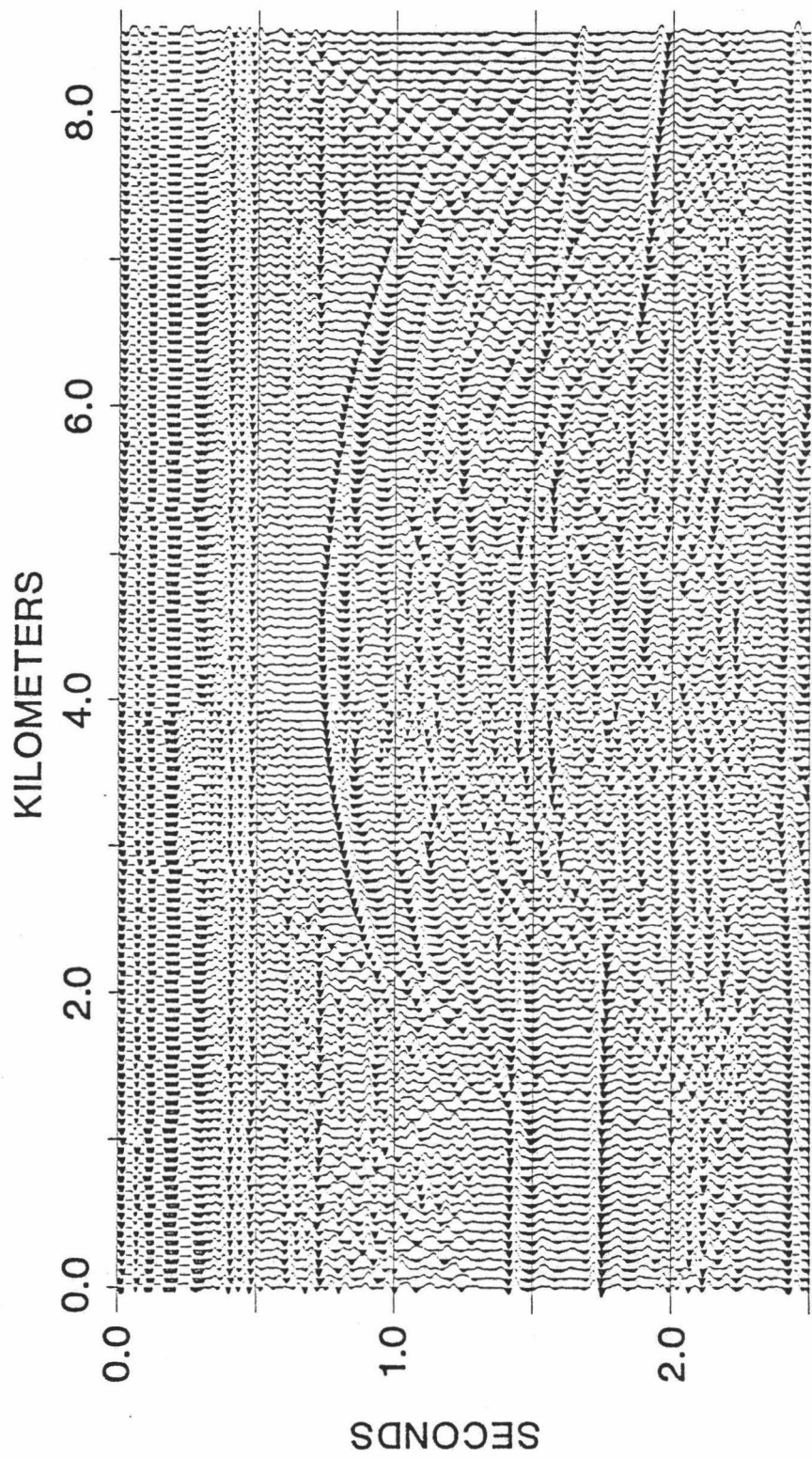
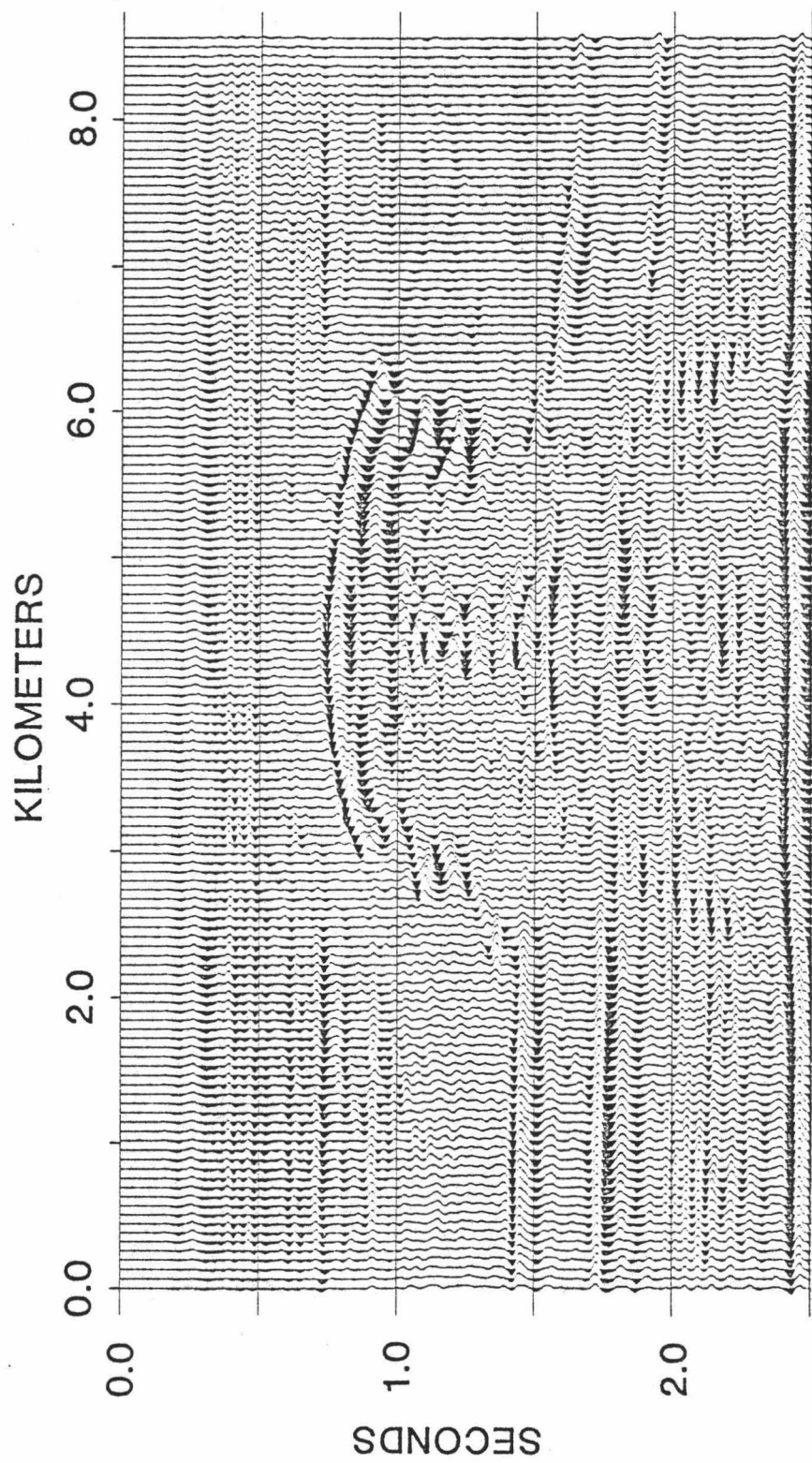


Figure 7



(a)

Figure 8a



(b)

Figure 8b